Detailed spectroscopy of ^{195}Bi

A. Herzáň,[1,2,*] S. Juutinen,[2] K. Auranen,[2,†] T. Grahn,[2] P. T. Greenlees,[2] K. Hauschild,[2,‡] U. Jakobsson,[2,3,§] R. Julin,[2] S. Ketelhut,[2] M. Leino,[2] A. Lopez-Martens,[2,‡] T. Lönnroth,[4] P. Nieminen,[2,∥] M. Nyman,[2,¶] J. Partanen,[2] P. Peura,[2,5] P. Rahkila,[2] P. Ruotsalainen,[2,6] M. Sandzelius,[2] J. Sarén,[2] C. Scholey,[2] J. M. K. Slotte,[4] J. Sorri,[2] S. Stolze,[2] and J. Uusitalo[2]

[1]*Oliver Lodge Laboratory, University of Liverpool, Liverpool L69 7ZE, United Kingdom*
[2]*University of Jyvaskyla, Department of Physics, P.O. Box 35, FI-40014 University of Jyvaskyla, Finland*
[3]*Department of Physics, KTH-Royal Institute of Technology, SE-10691 Stockholm, Sweden*
[4]*Physics, Faculty of Science and Engineering, Åbo Akademi University, FI-20500 Turku, Finland*
[5]*Helsinki Institute of Physics, University of Helsinki, P.O. Box 64, 00014 Helsinki, Finland*
[6]*TRIUMF, Westbrook Mall, Vancouver, British Columbia, Canada V6T 2A3*

An experiment focused on the study of shape coexistence and new high-spin structures in ^{195}Bi has been performed. The nucleus is in a transitional region of the bismuth isotope chain. A large number of new states have been found, resulting in a significant extension of the previously known level scheme. Several new collective structures have been identified. A strongly coupled rotational band built upon the $13/2^+$ isomeric state was extended up to $I^\pi = (49/2^+)$ and an energy of 5706 keV. The $I^\pi = 31/2^+$ member of the $\pi i_{13/2}$ band was also found to feed a new long-lived isomeric state with an excitation energy of 2616 keV and a spin and parity of $I^\pi = 29/2^+$. The half-life of the $29/2^+$ isomeric state was determined to be 1.49(1) μs. It decays via the emission of 457-keV $E2$ and 236-keV $E1$ transitions, respectively. A low-energy 46-keV $E2$ transition has been identified to depopulate the $(29/2^-)$ isomeric state, with a measured half-life of $T_{1/2} = 614(5)$ ns. This transition allows the excitation energy of the isomeric state to be determined as 2381 keV. The feeding patterns of both $29/2^+$ and $(29/2^-)$ isomeric states have also been described. This is the first time collective structures have also been observed up to high spins and excitation energies in the neutron-deficient ^{195}Bi nucleus. Evidence for the manifestation of shape coexistence in ^{195}Bi is also discussed.

I. INTRODUCTION

Bismuth nuclei close to neutron number $N \approx 110$ form a transitional region between spherical and deformed isotopes. In ^{191}Bi and ^{193}Bi, rotational bands have been revealed [1–3]. The oblate 13/2[606] Nilsson orbital has been associated with the strongly coupled rotational bands built upon the isomeric $13/2^+$ states in both nuclei. Negative parity strongly coupled bands associated with the 7/2[514] configuration have been observed. In the recent work [3] several other rotational level sequences as well as level structures associated with spherical shape were identified in ^{193}Bi. Furthermore, two high-spin isomeric states with $I^\pi = (29/2^-)$ and $29/2^+$ were placed close to 2.3 MeV, separated by only 55 keV. In the heavier Bi isotopes spherical structures are expected to become more dominant.

In addition to spherical and weakly deformed oblate shapes, superdeformed bands have also been observed in several Bi isotopes [1,3–5]. To date, the only heavier nucleus with an experimentally observed superdeformed band is ^{198}Po [6,7] with $Z = 84$. In the odd-mass Bi nuclei, the configuration of superdeformed bands can be thought of in terms of an unpaired proton coupled to the even-even Pb superdeformed core. These bands in odd $A = 191$–197 nuclei are best interpreted when the proton is assumed to be in the $i_{11/2}1/2^+$[651] orbital [8,9].

Regarding knowledge of the structure of ^{195}Bi, only limited information was available until the present study. First, Lönnroth *et al.* [10] reported on the observation of the yrast states up to $I^\pi = (27/2^+)$ and showed evidence for a high-spin isomeric state above 2.3 MeV with a half-life of 750 ns. More recent works [11,12] report on the discovery of a new isomeric state having a spin and parity of $(31/2^+)$ and half-life 1.5(1) μs, along with a collective level structure above the $13/2^+$ isomeric state.

In this work, the level structure of ^{195}Bi was studied using the JUROGAM II germanium detector array and the RITU gas-filled recoil separator. A rather complicated level scheme with both spherical and deformed level structures including a strongly coupled band associated with the oblate proton 13/2[606] configuration was constructed. Two high-spin isomeric states were firmly established and assigned spins and parities of $I^\pi = (29/2^-)$ and $29/2^+$, respectively. The $(29/2^-)$ isomeric state is strongly populated and the level structure feeding it is found to be far more complicated when compared to ^{193}Bi. The excitation energies of the $29/2^+$

———————
*andrej.herzan@liverpool.ac.uk

[†]Present address: Argonne National Laboratory, 9700 Cass Ave, Lemont, IL 60439, USA.

[‡]Present address: CSNSM, IN2P3-CNRS, F-91405 Orsay Campus, France.

[§]Present address: Laboratory of Radiochemistry, Department of Chemistry, P.O. Box 55, FI-00014 Univeristy of Helsinki, Finland.

[∥]Present address: Fortum Oyj, Power Division, P.O. Box 100, 00048 Fortum, Finland.

[¶]Present address: European Commission, Joint Research Centre, IRMM, Retieseweg 111, B-2440 Geel, Belgium.

isomeric states in ^{193}Bi and ^{195}Bi follow the trend of the $13/2^+$ states. One band with features associated with superdeformed bands was observed.

II. EXPERIMENTAL DETAILS

The experiment was carried out at the Accelerator Laboratory of the University of Jyväskylä (JYFL), Finland, in two phases. The ^{195}Bi nuclei were produced in the fusion-evaporation reaction ^{159}Tb(^{40}Ar,4n)^{195}Bi. In the first phase of the experiment, a thin ^{159}Tb target deposited on a C foil was bombarded with a ^{40}Ar beam, accelerated to an energy of 175 MeV by the $K = 130$ MeV cyclotron. The average beam current was 9 pnA. In this phase the RITU gas-filled recoil separator was used to allow recoil tagging of γ rays, and study long-lived isomeric states. In the second phase JUROGAM II was used in a stand-alone experiment. A thick Au layer was used as a backing for the Tb target in order to stop the fusion-evaporation products at the target position. The beam energy optimized for production of ^{195}Bi nuclei remained the same, whereas beam current was decreased to an average value of 3 pnA. In general, backed target experiments can be used to study short-lived isomeric states. In the present experiment, only isomeric states with half-lives longer than $\sim$90 ns could be studied at the target position, as the time resolution of the JUROGAM II array was found to be of the order of 80–90 ns, depending on the energy of the incident γ ray.

The JUROGAM II High-Purity Germanium (HPGe)-detector array was used to detect prompt γ rays at the target position. The array consisted of 24 Clover [13] and 15 Eurogam Phase1 [14] or GASP [15] Compton-suppressed HPGe detectors. These detectors were instrumented with Lyrtech VHS-ADC cards, which allowed direct digitization of the preamplifier signals. The energies of detected γ rays were determined using a moving window deconvolution (MWD) algorithm [16] implemented in the FPGA of the ADC cards. The total photopeak efficiency of JUROGAM II using the add-back technique was 5.2% at 1.3 MeV. The JUROGAM II array was coupled to the helium-gas-filled recoil separator RITU [17,18] to separate the nuclei of interest from unwanted particles. The ions were subsequently analyzed using the GREAT focal plane spectrometer [19]. The fusion products of interest (recoils, Re) were identified based on the energy loss in a multiwire proportional counter (MWPC) and the time-of-flight (ToF) between MWPC and two double-sided silicon strip detectors (DSSDs). The two 300-μm-thick DSSD detectors were 40 mm $\times$ 60 mm in size with a 1-mm strip pitch, placed side by side. In this experiment, the DSSDs were used for recoil implantation and for detection of their subsequent decays such as α decay in horizontal strips (DSSD-Y side) or internal conversion electrons in vertical strips (DSSD-X side) [19]. Silicon PIN diode detectors were mounted in a box arrangement upstream from the DSSD to detect α particles and conversion electrons which may escape from the DSSDs. A planar germanium detector was placed directly behind the DSSDs to detect low-energy γ rays and x rays. High-energy γ rays emitted at the focal plane of RITU were detected by a set of three clover HPGe detectors mounted around the GREAT spectrometer on either side and from above.

The data from all electronics channels were recorded synchronously using the triggerless Total Data Readout (TDR) [20] data acquisition system. All the events were time stamped with 10 ns precision. The data were analyzed using the recoil-gating and isomer-tagging techniques [21], and processed using the GRAIN [22] and RADWARE [23,24] software packages.

III. RESULTS

Two α-decaying states are known in ^{195}Bi. The $9/2^-$ ground state [$E_\alpha = 5420(5)$ keV and $E_\alpha = 5713(5)$ keV, a total $b_\alpha = 0.03\%$, $T_{1/2} = 160(11)$ s], and the $1/2^+$ proton intruder state located at an excitation energy E_{ex} of 410 keV [$E_\alpha = 6106(5)$ keV, $b_\alpha = 33\%$, and $T_{1/2} = 87(1)$ s] [25]. The long half-lives in combination with small α-decay branches mean that a recoil-decay tagging (RDT) [26] analysis cannot be performed, as it is not possible to obtain clean recoil-α correlations.

Analysis of the experimental data was performed in a similar manner to that described in [3], with the same set of spectroscopic tools being applied. If not otherwise specified, a time window of 5 μs was used to search for delayed γ rays following the implantation of a recoil in the focal plane detector system. All the conclusions made in the following sections are verified by examination of γ-γ, and where possible, also γ-γ-γ coincidence data. As a result, many rotational bands and groups of transitions have been put together to create the complex level scheme for ^{195}Bi presented in Fig. 1. All the corresponding γ-ray transitions are listed in Tables I–III. Internal conversion coefficients extracted from the focal plane germanium and PIN diode detector data are listed in Table II and prove $M1$ and $E2$ character for the 391- and 422-keV transitions, respectively. It will be shown later that these transitions form an important key in the remaining data analysis. The results of the analysis of the focal plane data are presented in Fig. 2.

The JUROGAM II array was used to determine experimental angular distribution ratios R_{expt} (DCO, directional correlation from oriented nuclei [27]) and linear polarization asymmetry factors A_P (IPDCO, integrated polarizational-directional correlation from oriented nuclei [28]) of prompt γ rays. For more details on both techniques using the JUROGAM II array, see [3]. Based on the experimental results obtained in this work, typical values of R_{expt} for stretched dipole and quadrupole transitions are 0.8 and 1.3, respectively. R_{expt} values for $\Delta I = 0$ transitions are similar to those for stretched quadrupole transitions. In the case of A_P, stretched magnetic transitions have a value of $A_P \sim -0.1$ and those of stretched electric transitions of $\sim$0.1. The resulting R_{expt} and A_P values with the error estimates are listed in Table III.

A. The $29/2^-$ isomeric state

In the study of ^{195}Bi performed by Lönnroth *et al.* [10], the existence of an isomeric state with $T_{1/2} = 750$ ns was inferred. It was postulated that this isomeric state lies above 2311 keV. On the basis of the systematic behavior of high-spin states in heavier odd-A Bi isotopes, the isomeric state was assigned a

FIG. 1. Level scheme of ^{195}Bi deduced in the present work. The widths of the transitions are proportional to the intensities in the recoil-gated JUROGAM II data. Among other quantities, the half-lives of the isomeric states are also shown.

FIG. 1. (*Continued.*)

suggested spin and parity of $29/2^-$. Additionally, Pai *et al.* [11] placed a low-energy 86-keV $E2$ transition connecting the

$29/2^{(-)}$ isomeric state to the $25/2^-$ state. This finding placed the $29/2^{(-)}$ isomeric state at an excitation energy of 2396 keV. Only recently, Roy *et al.* [12] reported a new measured half-life of 0.7(1) μs for the $29/2^{(-)}$) isomeric state.

TABLE I. Transition energies (E_γ), relative intensities ($I_{\gamma(\mathrm{FP})}$) in the recoil-gated focal plane planar or clover (*) spectra, multipolarities, theoretical internal conversion coefficients (ICC$_{\mathrm{th}}$) [29], and the total transition intensities of selected γ-ray transitions below the $29/2^+$ and $29/2^-$ isomeric states in ^{195}Bi. The $I_{\gamma(\mathrm{FP})}$ and $I_{\mathrm{Tot.}}(\mathrm{FP})$ values have been normalized with respect to the 421.8-keV transition. A systematic error of about 0.3 keV should be added to the fitting errors given for most of the transitions listed in the first column. $I_{\mathrm{Tot.}}(\mathrm{FP})$ of the 32-keV transition is estimated based on the intensity balance and total intensity of the 659.4-keV transition.

E_γ (keV)	$I_{\gamma(\mathrm{FP})}$(%)	Multipolarity	ICC$_{\mathrm{th}}$	$I_{\mathrm{Tot.}}$(FP)
Gate: 434 + 454 keV				
(25.0(5))		$M1$	111.9(16)	<43
32.0(5)		$E2$	1551(22)	~13
55.0(2)	3.8(3)	$E1$	0.472(7)	5.3(4)
90.0(2)	4.3(3)	$E2$	10.34(15)	~47(3)
114.8(1)	14(1)	$E2$	3.75(6)	65(4)
140.2(1)	12(1)	$M1$	3.90(6)	55(3)
150.6(1)	92(5)	$E1$	0.1575(22)	102(5)
176.0(1)	22(1)	$E1$	0.1095(16)	23(1)
236.0(2)	2.8(3)	$M1$	0.899(13)	5.0(6)
236.2(3)	0.5(1)	$M1$	0.899(13)	0.9(3)
343.8(1)	76(4)	$M1$	0.320(5)	96(6)
391.3(1)	70(4)	$M1$	0.226(4)	81(5)
421.8(1)	100(6)	$E2$	0.0468(7)	100(6)
488.8(2)	3(1)	$E2$	0.0324(5)	3(1)
600.8(1)	51(1)*	$E2$	0.0201(3)	50(1)
659.4(2)	14(1)*	$E2$	0.01639(23)	13(1)
Gate: 620 + 624 keV				
114.8(1)	22(1)	$E2$	3.75(6)	101(6)
235.8(2)	6.1(5)	$E1$	0.0536(8)	6.1(5)
343.8(1)	75(4)	$M1$	0.320(5)	95(6)
391.3(1)	82(5)	$M1$	0.226(4)	95(6)
421.8(1)	100(6)	$E2$	0.0468(7)	100(6)
457.1(3)	95(6)	$E2$	0.0382(6)	95(6)

In the present study, the existence of the $(29/2^-)$ isomeric state is confirmed by the analysis of the focal plane data. However, the presence of a delayed 86-keV transition is

TABLE II. Transition energies (E_γ), K, and $L + M$ conversion coefficients [$\alpha_{K,\mathrm{expt}}(\mathrm{FP})$ and $\alpha_{L+M,\mathrm{expt}}(\mathrm{FP})$] obtained from focal plane recoil-gated germanium and PIN diode spectra, theoretical K and $L + M$ conversion coefficients ($\alpha_{K,\mathrm{th}}$ and $\alpha_{L+M,\mathrm{th}}$) [29], and multipolarity of the selected γ-ray transitions below the $29/2^+$ and $29/2^-$ isomeric states in ^{195}Bi. A systematic error of about 0.3 keV should be added to the fitting errors given for most of the transitions listed in the first column.

E_γ (keV)	$\alpha_{K,\mathrm{expt}}$ (FP)	$\alpha_{L+M,\mathrm{expt}}$ (FP)	$\alpha_{K,\mathrm{th}}$	$\alpha_{L+M,\mathrm{th}}$	Multipolarity
343.8(1)			0.261(4)		$M1$
391.3(1)	0.177(31)		0.183(3)		$M1$
421.8(1)	0.030(9)	0.014(6)	0.0308(5)	0.0151(2)	$E2$
457.1(3)	0.027(11)		0.0259(4)		$E2$

excluded, as it is not observed in either the focal plane clover or in the planar germanium γ-ray spectra.

Inspection of the focal plane germanium detector spectra revealed new transitions with energies of 140 and 176 keV. Since transitions with the same energies are also seen in the JUROGAM II spectra from the target position, they cannot directly depopulate the $(29/2^-)$ isomeric state. However, the measured intensities are much lower than the intensities of the 391- and 422-keV transitions in the JUROGAM II spectra. The 140-keV $M1$ transition is determined as depopulating the $23/2^+$ state placed at 2.184 MeV. The 176-keV transition is identified to feed the $25/2^+$ state at an excitation energy of 2.159 MeV in the present level scheme (see Fig. 1). The $25/2^+$ state is depopulated by a 115-keV $E2$ transition.

Several new low-energy transitions are also observed in the analysis of the prompt-delayed γ-γ coincidences. In the JUROGAM II singles spectra, a strong 454-keV γ-ray transition appears. This transition is found to be in prompt coincidence with another, rather strong transition with an energy of 434 keV. Figure 3(a) shows the spectrum of γ rays measured in the focal plane planar germanium detector and gated on the prompt 434- and 454-keV transitions observed in JUROGAM II. Among other strong transitions in this spectrum, γ-ray transitions with energies of 55, 90, 115, 140, 151, and 176 keV can be seen. In the analysis of the delayed γ-γ coincidences, the 140- and 151-keV transitions, together with the 176- and 115-keV transitions, are found to form two parallel paths feeding the $21/2^+$ state of Group C (Fig. 1). Taking into account the total transition intensities (see Table I) of all the transitions involved in this feeding pattern (see Fig. 2), it can be seen that assuming an $E1$ character for both the 151- and 176-keV transitions results in an excellent intensity ratio within the feeding pattern. Furthermore, the results of the DCO analysis are in agreement with the stretched 151-keV $\Delta I = 1$ $E1$ transition and 176-keV $\Delta I = 0$ $E1$ transition, thus supporting a negative parity assignment for the $I = 25/2$ state placed at 2335 keV in our level scheme. Based on a comparison of the recoil-gated thin target data and the thick target data it is concluded that the $25/2^-$ state at an excitation energy of 2335 keV must also have an isomeric character.

The short half-life of this $25/2^-$ isomeric state cannot be extracted from the recoil-gated data of the present experiment, because the state is fed by a transition depopulating another isomeric state with a much longer half-life.

In addition, the γ-γ coincidence data from the thick target part of the experiment also do not provide a clean decay curve for low-energy transitions, due to the γ-γ time resolution being of the order of ~80 ns. Lönnroth *et al.* [10], on the basis of a time-delay curve analysis, concluded that the 151-keV transition depopulates an isomeric state with a half-life of $T_{1/2} \approx 80$ ns. This half-life is adopted for the $25/2^-$ state at 2335-keV de-exciting by emission of the 151-keV γ-ray.

When gating with the prompt 454-keV transition feeding the $(29/2^-)$ isomeric state in the delayed-prompt γ-γ coincidence matrix, transitions of Band 2 are clearly visible. In Fig. 3(b), the planar Ge-detector spectrum gated on the 601-keV transition, feeding Band 2, in the delayed γ-γ matrix is shown. In this spectrum, the 90-keV γ-ray transition is present. In the level scheme, the 90-keV transition is placed

TABLE III. Energies E_γ, relative intensities (obtained from JUROGAM II data) I_γ, excitation energies E_i, and initial and final spins I_i^π and I_f^π, respectively, for the γ-ray transitions assigned to ^{195}Bi. Also angular distribution ratios R_{expt}, linear polarization asymmetry factors A_P, and multipolarities are shown. The intensities have been normalized with respect to the 343.8-keV $15/2^+ \rightarrow 13/2^+$ transition. The systematic error of about 0.3 keV should be added to the fitting errors given for most of the transitions listed in the first column.

E_γ (keV)	I_γ (%)	E_i (keV)	I_i^π	I_f^π	R_{expt}	A_P	Multipolarity
Band 1							
54.5(5)[a]		887	$13/2^+$	$11/2^-$			*E1*
67.0(5)		3048	$27/2^+$	$25/2^+$			*M1*
74.0(5)[b]		3123	$29/2^+$	$27/2^+$			*M1*
112.5(1)	24(1)	3236	$31/2^+$	$29/2^+$	0.75(9)		*M1*
156.2(1)	81(3)	3392	$33/2^+$	$31/2^+$	0.68(6)		*M1*
156.6(1)	40(2)	3048	$27/2^+$	$25/2^+$	0.60(6)		*M1*
211.6(1)	111(5)	3604	$35/2^+$	$33/2^+$	0.71(6)		*M1*
231.9(1)	13(1)	3123	$29/2^+$	$25/2^+$	0.96(12)		*E2*
249.4(1)	115(4)	3853	$37/2^+$	$35/2^+$	0.68(6)		*M1*
(274.5(1))	20(1)	(5065)	$(45/2^+)$	$(43/2^+)$	0.67(8)		*(M1)*
288.2(1)	100(4)	4141	$39/2^+$	$37/2^+$	0.63(7)		*M1*
(292.3(2))	16(1)	(5358)	$(47/2^+)$	$(45/2^+)$			*(M1)*
307.7(1)	267(10)	1538	$17/2^+$	$15/2^+$	0.70(6)	$-0.037(2)$	*M1*
311.7(1)	76(3)	4453	$41/2^+$	$39/2^+$	0.83(13)		*M1*
325.9(1)	92(4)	2891	$25/2^+$	$23/2^+$	0.76(7)		*M1*
332.3(1)	136(5)	2208	$21/2^+$	$19/2^+$	0.71(7)		*M1*
337.0(1)	183(7)	1875	$19/2^+$	$17/2^+$	0.75(7)		*M1*
338.2(1)	52(3)	4791	$43/2^+$	$41/2^+$	0.76(7)		*M1*
343.8(1)	1000(50)	1231	$15/2^+$	$13/2^+$	0.84(6)		*M1*
(348.2(3))	14(2)	(5706)	$(49/2^+)$	$(47/2^+)$	0.87(22)		*M1+E2*
358.1(1)	83(4)	2565	$23/2^+$	$21/2^+$	0.73(5)		*M1*
368.2(3)	14(1)	3604	$35/2^+$	$31/2^+$	1.3(3)		*E2*
460.7(2)	12(2)	3853	$37/2^+$	$33/2^+$			*E2*
482.2(2)	11(1)	3048	$27/2^+$	$23/2^+$	1.32(23)		*E2*
537.4(1)	35(2)	4141	$39/2^+$	$35/2^+$	1.59(17)		*E2*
599.7(1)	41(2)	4453	$41/2^+$	$37/2^+$			*E2*
(612.5(2))	9(1)	(5065)	$(45/2^+)$	$41/2^+$			*(E2)*
644.7(1)	99(4)	1875	$19/2^+$	$15/2^+$	1.32(10)	0.059(4)	*E2*
649.6(2)	17(2)	4791	$43/2^+$	$39/2^+$			*E2*
651.5(1)	111(5)	1538	$17/2^+$	$13/2^+$	1.24(12)		*E2*
669.2(1)	110(5)	2208	$21/2^+$	$17/2^+$	1.19(11)		*E2*
683.7(1)	114(4)	2891	$25/2^+$	$21/2^+$	1.17(12)		*E2*
690.2(1)	69(3)	2565	$23/2^+$	$19/2^+$	1.23(13)		*E2*
886.6(1)[a]		887	$13/2^+$	$9/2^-$			*M2*
Band 2							
116.1(2)	3.6(7)	950	$13/2^-$	$11/2^-$			*M1*
224.4(1)	23(1)	1644	$17/2^-$	$15/2^-$	0.66(10)		*M1*
236.2(3)	6.2(1)	2303	$21/2^-$	$19/2^-$			*M1*
423.1(1)	51(2)	2067	$19/2^-$	$17/2^-$	0.69(10)		*M1*
425.2(2)	13(2)	2729	$23/2^-$	$21/2^-$			*M1*
469.8(1)	97(4)	1419	$15/2^-$	$13/2^-$	0.70(9)		*M1*
586.7(1)	113(4)	1419	$15/2^-$	$11/2^-$	1.33(13)		*E2*
647.5(1)	78(3)	2067	$19/2^-$	$15/2^-$	1.14(13)		*E2*
659.4(3)	77(4)	2303	$21/2^-$	$17/2^-$	1.3(2)		*E2*
661.3(1)	37(2)	2729	$23/2^-$	$19/2^-$	1.23(21)		*E2*
693.9(1)	219(8)	1644	$17/2^-$	$13/2^-$	1.11(11)		*E2*
832.8(1)	174(7)	833	$11/2^-$	$9/2^-$	0.67(8)		*M1*
949.8(1)	421(31)	950	$13/2^-$	$9/2^-$	1.32(11)	0.039(22)	*E2*
Band 3							
114.8(1)	19(1)	2159	$25/2^+$	$21/2^+$	1.13(8)		*E2*
283.9(3)	5.6(7)	3710		$31/2^+$			
334.4(3)	5.1(7)	3057	$29/2^+$	$27/2^+$			*M1*
(360.2(3))	5.0(8)	(4071)					

TABLE III (*Continued.*)

E_γ (keV)	I_γ (%)	E_i (keV)	I_i^π	I_f^π	R_{expt}	A_P	Multipolarity
369.2(1)	15(1)	3426	$31/2^+$	$29/2^+$	0.6(1)		*M1*
563.6(1)	32(1)	2723	$27/2^+$	$25/2^+$	0.59(8)		*M1*
(644.6(2))	9.4(9)	(4071)		$31/2^+$			
652.6(2)	9(1)	3710		$29/2^+$			
703.6(1)	11(1)	3426	$31/2^+$	$27/2^+$	1.28(25)		*E2*
897.9(1)	21(1)	3057	$29/2^+$	$25/2^+$	1.57(23)		*E2*
Band 4							
(46.0(5))[c]		2381	$(29/2^-)$	$25/2^-$			(E2)
260.1(1)	32(1)	3902	$(37/2^-)$	$(35/2^-)$	0.82(9)		*M1*
329.2(1)	21(1)	4592	$(41/2^-)$	$(39/2^-)$			*M1*
361.1(1)	36(2)	4263	$(39/2^-)$	$(37/2^-)$	0.82(11)		*M1*
373.9(1)	100(3)	3642	$(35/2^-)$	$(33/2^-)$	0.70(7)		*M1*
388.8(1)	19(1)	4981	$(43/2^-)$	$(41/2^-)$			*M1*
434.1(1)	201(7)	3268	$(33/2^-)$	$(31/2^-)$	0.60(6)		*M1*
453.6(1)	601(20)	2384	$(31/2^-)$	$(29/2^-)$	0.64(6)		*M1*
620.8(1)	27(2)	4263	$(39/2^-)$	$(35/2^-)$	1.21(18)		*E2*
633.5(1)	41(2)	3902	$(37/2^-)$	$(33/2^-)$	1.33(15)		*E2*
691.3(1)	21(1)	4592	$(41/2^-)$	$(37/2^-)$	1.5(3)		*E2*
718.3(1)	14(1)	4981	$(43/2^-)$	$(39/2^-)$	1.4(3)		*E2*
807.5(1)	31(2)	3642	$(35/2^-)$	$(31/2^-)$	1.37(20)		*E2*
888.0(1)	71(4)	3268	$(33/2^-)$	$(29/2^-)$	1.23(15)		*E2*
Band 5							
123.9(1)	77(18)		$i+1$	i	0.9(1)		*M1+E2*
192.9(1)	8.3(6)		$i+2$	$i+1$	1.15(13)		*M1+E2*
198.6(2)	5.7(6)		$i+2$	$i+1$			*M1*
250.2(1)	30(1)		$i+8$	$i+7$	0.84(9)		*M1*
255.3(1)	49(2)		$i+3$	$i+2$	0.75(8)		*M1*
261.6(1)	78(3)		$i+3$	$i+2$	0.72(9)		*M1*
286.4(1)	109(4)		$i+4$	$i+3$	0.7(1)		*M1*
307.2(1)	90(3)		$i+5$	$i+4$	0.74(8)		*M1*
315.4(1)	85(3)		$i+6$	$i+5$	0.86(9)		*M1*
(348.6(1))	1(1)		$i+1$	$i+1$			(M1)
395.6(1)	21(1)		$i+9$	$i+8$	0.95(11)		*M1+E2*
399.5(1)	34(2)		$i+7$	$i+6$	0.59(7)		*M1*
410.3(1)	17(1)			$i+9$			
541.4(1)	77(5)		$i+2$	$i+1$	0.98(10)		*M1+E2*
547.7(1)	54(4)		$i+2$	$i+1$	0.66(8)		*M1*
548.0(1)	12(1)		$i+4$	$i+2$	1.36(36)		*E2*
557.7(1)	20(1)		$i+6$	$i+4$	1.24(18)		*E2*
593.6(1)	39(2)		$i+5$	$i+3$	1.1(2)		*E2*
622.6(1)	35(2)		$i+6$	$i+4$	1.06(11)		*E2*
665.6(1)	49(2)		$i+2$	i	1.46(16)		*E2*
671.9(1)	36(2)		$i+2$	i	1.39(19)		*E2*
716.5(2)	7.0(8)		$i+7$	$i+5$			*E2*
Band 6[d]							
169.0(2)	18(4)		$j+1$	j	0.88(14)		*M1+E2*
195.6(2)	16(2)		$j+2$	$j+1$	0.93(17)		*M1+E2*
228.9(2)	15(1)		$(j+3)$	$j+2$			(M1)
268.4(1)	11(1)		$(j+4)$	$(j+3)$	(0.92(17))		(M1)
294.3(2)	10(1)		$(j+5)$	$(j+4)$	(0.98(19))		(M1)
497.4(5)	3(1)		$(j+4)$	$j+2$	(1.46(31))		(E2)
562.7(4)	5(2)		$(j+5)$	$(j+3)$	(1.6(3))		(E2)
Group A							
115.9(1)	9.5(7)	2845					
121.8(1)	12(1)	2729					
122.3(2)	6(1)	2521	$23/2^+$	$19/2^+$	1.25(10)		*E2*

TABLE III (*Continued.*)

E_γ (keV)	I_γ (%)	E_i (keV)	I_i^π	I_f^π	R_{expt}	A_P	Multipolarity
192.5(1)	11(1)	3037					
286.1(2)	12(1)	2607		$17/2^+$			
(399.6(8))	3(1)	(3007)					
435.9(2)	21(2)	2243	$19/2^+$	$17/2^+$	0.73(6)		*M1*
576.6(1)	89(4)	1807	$17/2^+$	$15/2^+$	0.67(7)		*M1*
591.5(1)	33(2)	2399	$19/2^+$	$17/2^+$	0.61(6)		*M1*
901.6(1)	21(2)	2321	$17/2^+$	$15/2^-$			*E1*
920.9(1)	46(4)	1807	$17/2^+$	$13/2^+$	1.52(13)		*E2*
1090.1(1)	56(3)	2321	$17/2^+$	$15/2^+$	0.85(11)		*M1*
Group B							
163.6(1)	11(1)	2523	$23/2^+$	$21/2^+$	1.1(2)		*M1+E2*
236.0(2)	36(2)	2280	$23/2^+$	$21/2^+$	0.9(1)		*M1+E2*
264.1(3)	6.6(7)	2359	$21/2^+$	$19/2^+$			*M1*
302.0(1)	10.5(6)	3595	$(33/2^+)$	$(29/2^+)$	0.7(1)		*(E2)*
315.7(1)	25(2)	2523	$23/2^+$	$21/2^+$	0.67(8)		*M1*
374.3(1)	45(2)	1996	$21/2^+$	$17/2^+$	1.17(14)		*E2*
381.1(1)	19(1)	2830	$27/2^+$	$23/2^+$	1.5(2)		*E2*
459.7(1)	9.5(7)	3293	$(29/2^+)$	$(27/2^+)$	0.9(2)		*(M1+E2)*
473.3(1)	43(2)	2095	$19/2^+$	$17/2^+$	0.75(12)		*M1*
511.3(1)	73(3)	2133	$19/2^+$	$17/2^+$	0.63(8)		*M1*
553.4(1)	11(1)	2833	$(27/2^+)$	$23/2^+$			*(E2)*
662.6(1)	28(2)	2285		$17/2^+$			
737.0(1)	35(3)	2359	$21/2^+$	$17/2^+$	1.28(18)		*E2*
Group C							
(25.0(5))[e]		2184	$23/2^+$	$25/2^+$			*M1*
83.0(5)[b]		1622	$17/2^+$	$17/2^+$			*M1*
140.2(1)	18(1)	2184	$23/2^+$	$21/2^+$	0.69(9)		*M1*
203.8(1)	15(1)	1622	$17/2^+$	$15/2^-$	0.64(13)		*E1*
311.7(2)	16(2)	1261	$13/2^+$	$13/2^-$	(0.85(14))		*E1*
360.6(3)	17(1)	1622	$17/2^+$	$13/2^+$	1.25(18)		*E2*
373.8(2)	33(6)	1261	$13/2^+$	$13/2^+$	(0.66(5))		*M1*
391.3(1)	530(17)	1622	$17/2^+$	$15/2^+$	0.83(7)	$-0.013(1)$	*M1*
404.9(1)	74(3)	2449	$23/2^+$	$21/2^+$	0.66(7)		*M1*
421.8(1)	406(13)	2044	$21/2^+$	$17/2^+$	1.16(9)	0.023(1)	*E2*
428.6(2)	22(2)	1261	$13/2^+$	$11/2^-$	0.83(13)		*E1*
506.8(1)	28(2)	2044	$21/2^+$	$17/2^+$	1.06(9)		*E2*
531.6(1)	31(1)	2980	$25/2^+$	$23/2^+$	0.66(7)		*M1*
577.1(1)	27(2)	2621	$23/2^+$	$21/2^+$	0.60(6)		*M1*
734.9(1)	66(4)	1622	$17/2^+$	$13/2^+$	1.06(15)		*E2*
796.3(1)	23(2)	2980	$25/2^+$	$23/2^+$	0.64(18)		*M1*
Group D							
197.2(1)	27(2)	690	$(9/2^-)$	$(7/2^-)$	0.67(8)		*(M1)*
219.6(2)	10(1)	1419	$15/2^-$	$13/2^-$	0.66(15)		*M1*
(286.7(4))	2.9(6)	(2574)		$15/2^-$			
336.4(1)	16(2)	1756	$17/2^-$	$15/2^-$	0.89(13)		*M1+E2*
366.2(1)	34(2)	1199	$13/2^-$	$11/2^-$	0.69(10)		*M1*
445.3(1)	18(1)	1644	$17/2^-$	$13/2^-$	1.43(29)		*E2*
469.3(3)	7(1)	1589	$(15/2^-)$				
492.3(1)	31(3)	492	$(7/2^-)$	$9/2^-$			*(M1)*
509.5(1)	38(2)	1199	$13/2^-$	$(9/2^-)$			*(E2)*
556.7(1)	24(2)	1756	$17/2^-$	$13/2^-$	1.14(21)		*E2*
613.8(1)	29(2)	2859		$21/2^-$			
623.6(2)	12(1)	3352		$23/2^-$			
(638.6(3))	11(2)	1589	$(15/2^-)$	$13/2^-$			*(M1)*
689.7(2)	29(4)	690	$(9/2^-)$	$9/2^-$			*(M1)*
695.1(2)	27(3)	2339	$21/2^-$	$17/2^-$	1.48(29)		*E2*
731.6(2)	16(1)	2799		$19/2^-$			

TABLE III (*Continued.*)

E_γ (keV)	I_γ (%)	E_i (keV)	I_i^π	I_f^π	R_{expt}	A_P	Multipolarity
734.1(1)	31(2)	1684	$15/2^-$	$13/2^-$	0.86(14)		*M1+E2*
755.8(2)	14(2)	1589	$(15/2^-)$	$11/2^-$	1.15(25)		*(E2)*
767.7(2)	12(1)	1967	$17/2^-$	$13/2^-$			*E2*
806.1(2)	21(2)	1756	$17/2^-$	$13/2^-$	1.32(32)		*E2*
1017.5(2)	15(2)	1967	$17/2^-$	$13/2^-$	1.27(34)		*E2*
1118.8(3)	9(1)	1119		$9/2^-$			
1199.3(1)	30(3)	1199	$13/2^-$	$9/2^-$	1.24(20)		*E2*
1337.2(1)	23(2)	2287	$15/2^-$	$13/2^-$	0.59(16)		*M1*
Group E							
152.5(1)	14(1)	3392	$33/2^+$	$31/2^+$	0.84(14)		*M1*
175.0(2)	3.5(4)	5018		$41/2^-$			
221.1(1)	11(1)	4843	$41/2^-$	$39/2^-$	0.95(18)		*M1+E2*
249.5(2)	6(1)	3893	$37/2^+$	$35/2^+$	0.62(11)		*M1*
278.2(1)	22(1)	3519	$33/2^+$	$31/2^+$	0.64(11)		*M1*
328.2(2)	8.4(7)	5618					
403.6(1)	25(2)	3644	$35/2^+$	$31/2^+$	1.24(18)		*E2*
526.1(2)	8.8(8)	5290		$41/2^+$			
538.7(1)	107(4)	4057	$37/2^+$	$33/2^+$	1.27(13)	0.099(12)	*E2*
557.7(1)	15(1)	4202		$35/2^+$			
564.7(1)	56(2)	4622	$39/2^-$	$37/2^+$	0.58(9)	0.055(8)	*E1*
(568.6(3))	7(1)	(3898)					
607.6(1)	32(2)	4126	$35/2^+$	$33/2^+$	0.83(19)		*M1*
620.2(1)	172(8)	3236	$31/2^+$	$29/2^+$	0.62(7)	−0.085(7)	*M1*
623.9(1)	88(6)	3240	$31/2^+$	$29/2^+$	0.81(16)	−0.109(20)	*M1*
664.4(1)	20(2)	3905		$31/2^+$			
706.6(1)	27(2)	4764	$41/2^+$	$37/2^+$	1.45(25)		*E2*
(712.6(3))	9(4)	(3329)					
902.3(1)	118(6)	3519	$33/2^+$	$29/2^+$	1.13(14)		*E2*
940.3(1)	10(2)	4459		$33/2^+$			
Group F							
129.6(1)	12(1)	3725	$(37/2^-)$	$(35/2^-)$	0.77(12)		*M1*
186.6(3)	6.0(5)	3595	$(35/2^-)$	$(33/2^-)$	0.54(15)		*M1*
228.9(1)	27(1)	3954	$(39/2^-)$	$(37/2^-)$	0.91(10)		*M1+E2*
231.6(4)	1.6(7)	3971	$(33/2^-)$	$(33/2^-)$			*(M1)*
233.2(1)	18(1)	3642	$(35/2^-)$	$(33/2^-)$	0.61(9)		*M1*
268.8(4)	3.7(8)	3548					
302.0(1)	53(2)	4256	$(41/2^-)$	$(39/2^-)$	0.94(10)		*M1+E2*
327.1(1)	33(1)	3595	$(35/2^-)$	$(33/2^-)$	0.91(11)		*M1+E2*
349.0(1)	36(2)	3991	$(37/2^-)$	$(35/2^-)$			*(M1)*
368.4(1)	23(2)	3850	$(35/2^-)$	$(33/2^-)$			*(M1)*
380.9(1)	20(1)	4637	$(43/2^-)$	$(41/2^-)$	0.84(14)		*M1*
400.2(1)	57(2)	4125	$(39/2^-)$	$(37/2^-)$	0.70(8)		*M1*
444.6(1)	21(2)	3279		$(31/2^-)$			
490.9(1)	22(1)	4482	$(39/2^-)$	$(37/2^-)$	0.5(1)		*M1*
574.6(1)	109(4)	3409	$(33/2^-)$	$(31/2^-)$	0.61(7)		*M1*
581.8(1)	20(1)	3991	$(37/2^-)$	$(33/2^-)$	1.24(18)		*E2*
647.6(1)	39(2)	3482	$(33/2^-)$	$(31/2^-)$	0.77(13)		*M1*
701.4(2)	14(1)	4344		$(35/2^-)$			
702.3(3)	8(1)	3971	$(33/2^-)$	$(33/2^-)$			*(M1)*
761.2(1)	111(4)	3595	$(35/2^-)$	$(31/2^-)$	1.1(1)		*E2*
778.0(2)	13(1)	4046		$(33/2^-)$			
839.6(1)	29(2)	4482	$(39/2^-)$	$(35/2^-)$			*(E2)*
905.6(2)	21(2)	3740	$(33/2^-)$	$(31/2^-)$	0.72(16)		*M1*
1016.1(2)	19(2)	3850	$(35/2^-)$	$(31/2^-)$	1.6(4)		*E2*
1101.2(2)	37(5)	3482	$(33/2^-)$	$(29/2^-)$			*(E2)*
1136.4(1)	23(2)	3971	$(33/2^-)$	$(31/2^-)$	0.64(13)		*M1*

TABLE III (*Continued.*)

E_γ (keV)	I_γ (%)	E_i (keV)	I_i^π	I_f^π	R_{expt}	A_P	Multipolarity
Other transitions							
32.0(5)[e]		2335	$25/2^-$	$21/2^-$			*E2*
55.0(2)[f]		2335	$25/2^-$	$23/2^+$			*E1*
90.0(2)[f]	16(9)	2335	$25/2^-$	$21/2^-$			*E2*
111.6(2)	6.4(7)	2982			0.98(22)		
150.6(1)	20(1)	2335	$25/2^-$	$23/2^+$	0.81(6)		*E1*
176.0(1)	8.3(7)	2335	$25/2^-$	$25/2^+$	1.25(9)		*E1*
234.3(3)	13(1)	3104			0.82(6)		
235.8(2)[g]		2616	$29/2^+$	$(29/2^-)$			*(E1)*
290.8(1)	12(1)	2536		$21/2^-$			
457.1(3)[h]		2616	$29/2^+$	$25/2^+$			*E2*
488.8(2)	13(3)	2245	$21/2^-$	$17/2^-$			*E2*
534.6(1)	14(1)	2870		$25/2^-$			
600.8(1)	137(8)	2245	$21/2^-$	$17/2^-$	1.21(13)		*E2*
167.5(5)[i]		$X + 167$	$(19/2^+)$	$(15/2^+)$			*(E2)*
209.5(5)[i]	3.7(9)	$X + 376$	$(23/2^+)$	$(19/2^+)$			*(E2)*
251.7(5)[i]	3.5(7)	$X + 628$	$(27/2^+)$	$(23/2^+)$			*(E2)*
293.1(5)[i]	5.7(7)	$X + 921$	$(31/2^+)$	$(27/2^+)$			*(E2)*
333.3(5)[i]	4.5(6)	$X + 1254$	$(35/2^+)$	$(31/2^+)$			*(E2)*
374.2(5)[i]	4.4(6)	$X + 1628$	$(39/2^+)$	$(35/2^+)$			*(E2)*
414.9(5)[i]	1.7(4)	$X + 2043$	$(43/2^+)$	$(39/2^+)$			*(E2)*

[a]γ-ray transition depopulating $13/2^+$ isomeric state. The extracted total intensity ratio is $I_{\mathrm{tot}}(54.5\,\mathrm{keV})/I_{\mathrm{tot}}(886.6\,\mathrm{keV}) = 0.05$.

[b]I_γ and R_{expt} could not be determined due to the strong contaminance of the peak by Bi K x-ray peak in the prompt γ-ray spectrum.

[c]γ-ray transition depopulating $(29/2^-)$ isomeric state.

[d]The intraband transitions seen in coincidence with lower-lying members of Band 4 (strong coincidences with the 454-keV transition).

[e]The transition energy is determined by the difference of the initial and final level energies.

[f]The transition is seen in the planar spectra.

[g]γ-ray transition depopulating $29/2^+$ isomeric state down to $(29/2^-)$ isomeric state. Transition seen in the focal plane data only.

[h]γ-ray transition depopulating $29/2^+$ isomeric state. Transition seen in the focal plane data only.

[i]γ-ray transitions seen in mutual coincidence in the recoil-gated prompt γ-γ-γ cube. The energies and energy spacings are similar to those of SD Band 2 in ^{196}Bi [5] and favorite signature SD bands in ^{191}Bi [1] and ^{193}Bi [3].

depopulating the $25/2^-$ isomeric state and feeding the 2245-keV $21/2^-$ state. This placement implies stretched $E2$ character for the 90-keV transition. A low-energy 32-keV $E2$ transition is also placed to depopulate the $I^\pi = 25/2^-$ isomeric state to the $I^\pi = 21/2^-$ state at 2303 keV (see Band 2 in Fig. 1), although it is not visible in the spectra of delayed transitions. The nonobservation of the 32-keV transition in the GREAT spectrometer is mainly due to the large internal conversion coefficient $\alpha_{Th.}(32\,\mathrm{keV}, E2) = 1551(22)$ [29], together with the high energy thresholds of the PIN diode detectors.

The 55-keV transition, observed when gating on the transitions feeding the isomer, is missing from Fig. 3(b).

Instead, a new low-energy transition with an energy of 46 keV is revealed. The transition intensity is however insufficient for any further analysis of its character. It is emphasized that this new transition is remarkably similar to a 49-keV transition placed as depopulating the $(29/2^-)$ isomeric state in ^{193}Bi [3]. Since no other γ-ray transitions are seen in Fig. 3(b), the 46-keV transition is tentatively associated with the decay of the $(29/2^-)$ isomeric state and placed to feed the short-lived $25/2^-$ isomeric state in ^{195}Bi. On the basis of energy sum arguments, the $(29/2^-)$ isomeric state is located at an excitation energy of 2381 keV in the level scheme (see Figs. 1 and 2). Subsequently, an $E2$ character for the 46-keV transition is assumed.
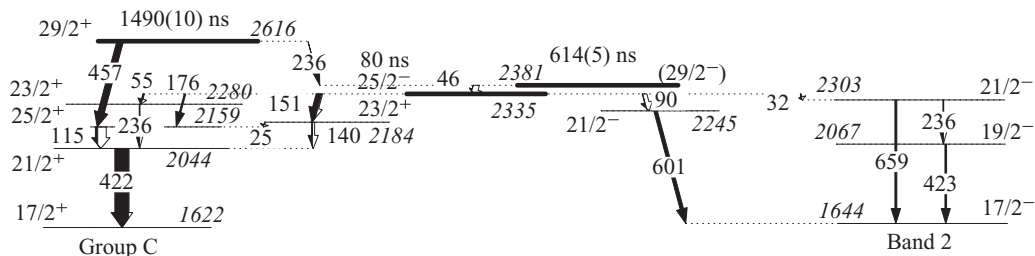

FIG. 2. Partial level scheme of ^{195}Bi, summarizing the depopulation of the $29/2^-$ and $29/2^+$ isomeric states.
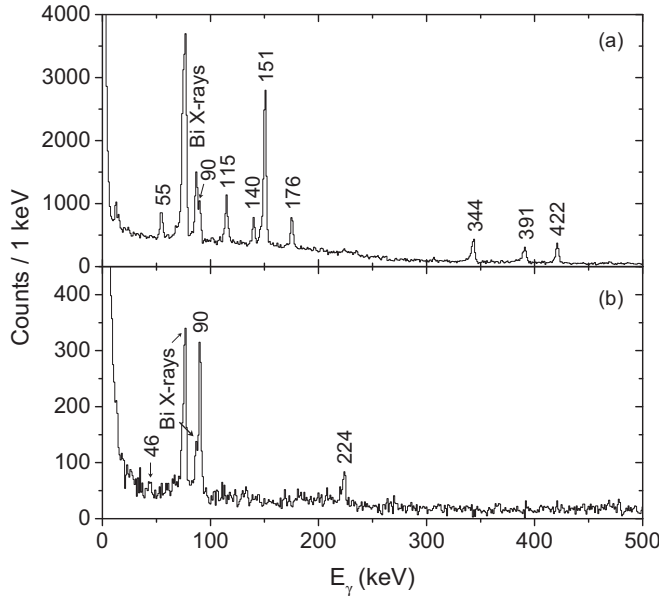
FIG. 3. γ-ray spectra measured in the planar Ge detector within 5 μs after the recoil implantation. (a) Sum of spectra gated with 434- and 454-keV prompt γ-ray transitions measured with JUROGAM II. (b) A spectrum gated with the 601-keV transition (Band 2) measured in focal plane Ge clover detector.

The half-life of the $(29/2^-)$ isomeric state is determined by projecting the time differences Δt (recoil-delayed γ) of the low-energy transitions located below the $25/2^-$ isomeric state. Figure 4(a) shows the time projection of the 151-keV γ-ray transition. Fitting the Δt distribution with an exponential decay function results in a half-life value of $T_{1/2} = 614(5)$ ns. Deviations of $T_{1/2}$ for other relevant transitions vary minimally and stay within the limit set by the uncertainty of the measured
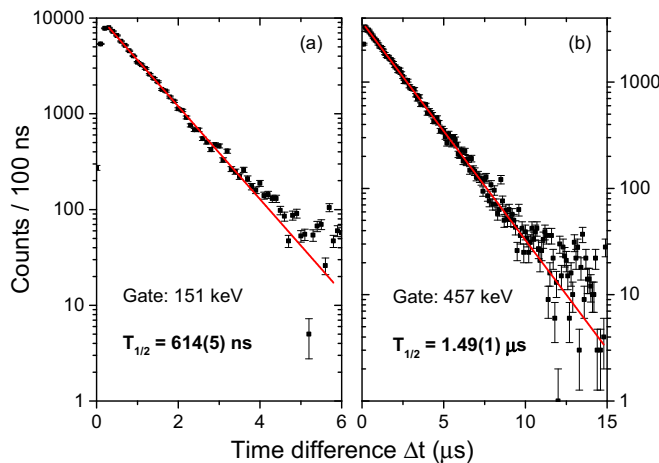
FIG. 4. Time difference spectra of the recoil implantation and observation of the (a) 151-keV and (b) 457-keV transitions, respectively. The exponential decay curve is fitted to the data and is shown as the solid line through data points. The background component was fitted separately. Both $T_{1/2}$ values are corrected for the background contribution.

half-life. This is in agreement with a half-life reported in [12] for the $29/2^{(-)}$ isomeric state.

Most of the observed decay paths of the $(29/2^-)$ isomeric state also proceed to Group C. By fitting the Δt time projections of the 391- and 422-keV transitions, respectively, half-lives longer than the one measured for the $(29/2^-)$ isomeric state are obtained. This is evidence for the existence of another, longer-lived isomeric state in this nucleus.

B. The $29/2^+$ isomeric state

In our recent study of ^{193}Bi [3], a high-spin isomeric state was observed to have a spin and parity of $29/2^+$ and was placed at an energy of 2350 keV. Its half-life was measured to be 85(3) μs. In another study performed by Roy *et al.* [12], the existence of a new high-spin isomeric state with a spin and parity of $I^\pi = (31/2^+)$ was postulated and placed at an excitation energy of 3336 keV in ^{195}Bi. Additionally, a delayed 238-keV $E2$ transition was associated with the decay of this isomeric state with a half-life of $T_{1/2} = 1.53(9)$ μs [12].

In the same study, Roy *et al.* [12] placed the 457-keV $M1$ transition as a member of the decay path of the $(31/2^+)$ isomeric state. In their level scheme [12], this transition is associated with the prompt decay of the $(23/2^+)$ level.

In the present data, the 457-keV transition is found to be among the strongest transitions observed in the focal plane γ-ray spectra. Furthermore, any association of this transition with the decay of the $(29/2^-)$ isomeric state is excluded. As shown in Fig. 3(a), no sign of a delayed 457-keV transition is found among transitions defining the decay path of the $(29/2^-)$ isomeric state. Figure 5(a) shows solely those γ-ray transitions, which are in prompt coincidence with the 457-keV γ-ray transition in the focal plane clover detectors. None of the low-energy transitions seen in Fig. 3(a) except the 115-keV transition is present in this spectrum. The 115-keV transition also appears in the focal plane clover spectrum gated on the 151-keV transition measured in the planar detector [see Fig. 5(b)]. In addition, it is worth mentioning that the 344-, 391-, and 422-keV transitions are present in all these focal plane spectra. Hence, the $25/2^+$ state at an energy of 2159 keV, de-exciting by emission of the 115-keV transition, must be a meeting point of the decay paths of two different isomeric states. Based on the aforementioned coincidences between delayed γ-ray transitions, the 457-keV transition is placed to depopulate the state at 2616 keV (see Fig. 1).

Figure 4(b) displays the fitted time projection of the 457-keV γ-ray transition. The resulting measured half-life is $T_{1/2} = 1.49(1)$ μs, which is clearly distinct from the half-lives of other isomeric states present in this nucleus. Our measured half-life matches well with the half-life of the $(31/2^+)$ isomeric state reported by Roy *et al.* [12].

To go further, contrary to the findings of Roy *et al.* [12], a spin and parity of $I^\pi = 29/2^+$ is deduced for the 1.49(1)-μs isomeric state. The excitation energy is determined to be 2616 MeV (see Fig. 1).

In order to illustrate the full decay path of this isomeric state, the spectrum measured in the focal plane clover detectors gated on the prompt 620- and 624-keV transitions is shown in Fig. 5(c). This spectrum contains the γ-ray transitions involved
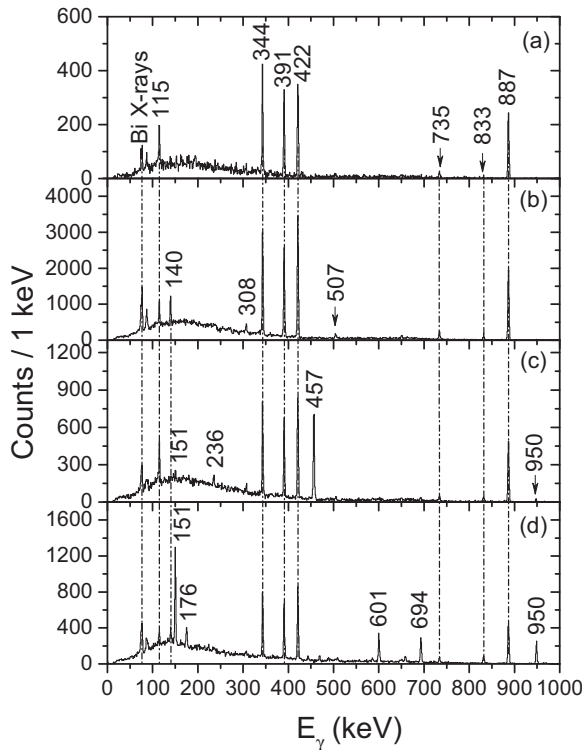
FIG. 5. A spectrum of delayed γ rays gated on the delayed (a) 457-keV and (b) 151-keV γ-ray transition and measured in the focal plane clover detector. Panels (c) and (d) show focal plane clover detectors spectra gated on the prompt 620- and 624-keV γ-ray transitions, and the 454-keV γ-ray transition, respectively, in the delayed-prompt γ-γ coincidence matrices.

in the decay path of the $29/2^+$ isomeric state. The composition of this spectrum is clearly different from the spectrum of delayed γ rays gated on the 454-keV transition feeding the $(29/2^-)$ isomeric state and shown in Fig. 5(d). No evidence for the presence of the 457-keV transition is found in Fig. 5(d). Analysis of the backed target data together with the measured internal conversion coefficients (see Table II) support an $E2$ character assignment for the 457-keV γ-ray transition. The 457-keV γ-ray transition is identified to directly depopulate the $29/2^+$ isomeric state to the 2159-keV $25/2^+$ state. The total transition intensities listed in Table I are in excellent agreement with the observed decay path of the $29/2^+$ isomeric state.

The energy difference between the $29/2^+$ and $(29/2^-)$ isomeric states is 236 keV, which allows the existence of an $E1$ transition measurable with our detection system. To complicate the identification of such a transition, one 236-keV $M1$ transition is already identified to be a part of the $(29/2^-)$ isomeric state decay path and to feed the $21/2^+$ state at an excitation energy of 2044 keV (Group C). A half-life of $T_{1/2} = 960$ ns is extracted for the 236-keV γ-ray transition from our data, which is longer than the half-life value of the $(29/2^-)$ isomeric state. By gating on the 620- and 624-keV transitions feeding the $29/2^+$ isomeric state in the delayed-prompt γ-γ coincidence matrices, a γ-ray peak with energy of 236 keV is indeed observed [see Fig. 5(c)]. Therefore, a linking 236-keV transition is placed between these two high-spin isomeric
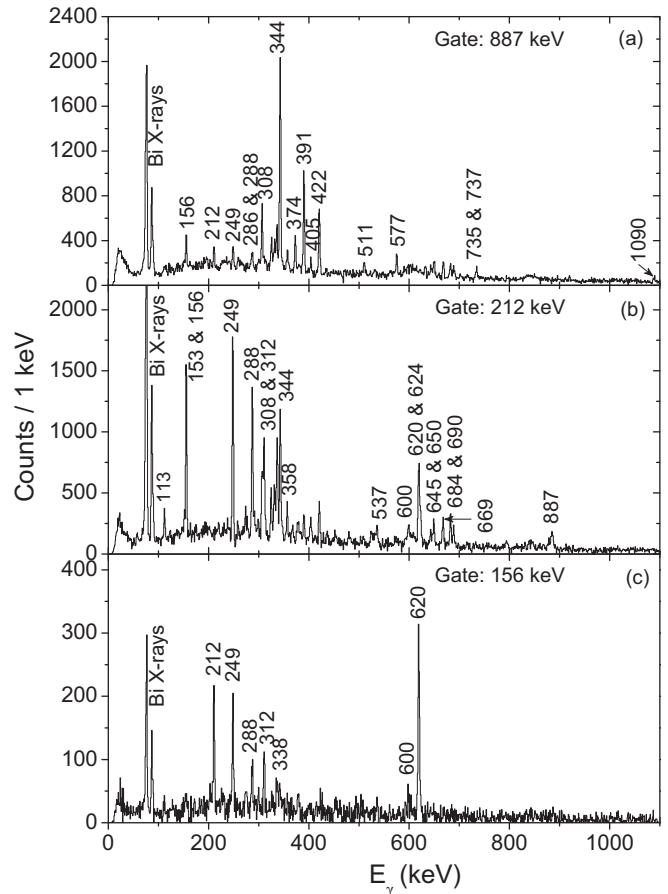
FIG. 6. An energy spectrum of prompt γ rays gated on the (a) 887-keV γ-ray transition and (b) 212-keV γ-ray transition. (c) An isomer-tagged JUROGAM II spectrum gated on the prompt 156-keV γ-ray transition in ^{195}Bi data.

states. No evidence for an additional decay path from the 2616-keV level is found.

C. Band 1: $i_{13/2}$

Lönnroth *et al.* [10] placed the delayed 888-keV $M2$ transition in the level scheme as feeding the $9/2^-$ ground state of ^{195}Bi. In their corresponding time-delay spectrum, a 32-ns time component was clearly observed. A spin and parity of $I^\pi = (13/2^+)$ was assigned to the 888-keV level. In the rather recent study of the ^{195}Bi nucleus by Pai *et al.* [11], the $13/2^+$ state at 887 keV was assigned to be a bandhead of a new rotational band.

In the present study, based on the analysis of prompt γ-γ coincidences, the observation in [10,11] that the 344-keV transition indeed feeds the short-lived $13/2^+$ isomeric state is confirmed. The DCO analysis for this transition suggests stretched $M1$ character. The short half-life $T_{1/2} = 32(2)$ ns of the $13/2^+$ isomeric state enables a gate to be placed on the 887-keV $M2$ transition in the JUROGAM II γ-ray spectrum. As can be seen in Fig. 6(a), the 344-keV transition clearly dominates. However, disagreements with both of the previously reported level schemes are found above the yrast
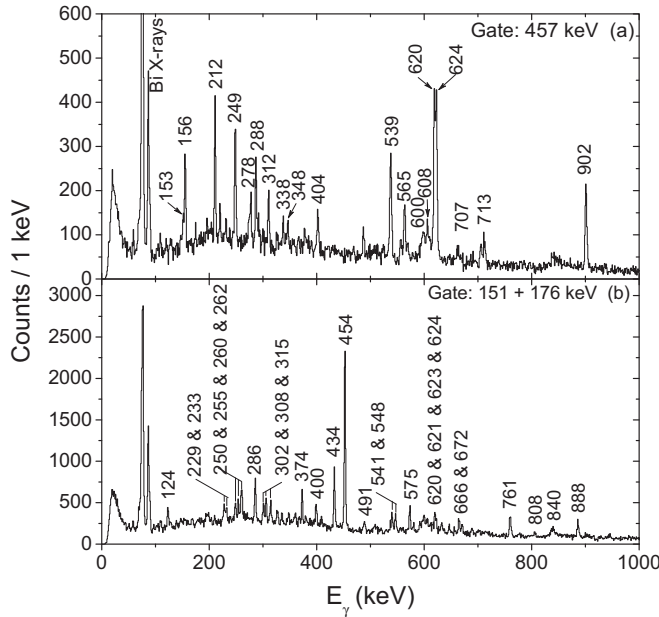
FIG. 7. A spectrum of prompt γ rays obtained when gating with (a) the 457-keV transition in the focal plane clover spectrum, and (b) the 151- and 176-keV transitions in the planar spectrum in ^{195}Bi experiment.

$I^\pi = 15/2^+$ state. Among other strong transitions visible in this spectrum, the majority of γ-ray transitions form Band 1 and feed the yrast $13/2^+$ state. The Band 1 level structure in [11] is however different when compared to the deduced level scheme shown in Fig. 1. Band 1 loses its yrast-band character between spins of $21/2 \leqslant I \leqslant 29/2$. Determination of the spins for the positive parity yrast states will be described in the following sections.

In the present study, the positive parity band feeding the $13/2^+$ bandhead (Band 1) is observed up to spin $I = (49/2)$ and an energy of 5706 keV. A sharp bandcrossing occurs above $I^\pi = 25/2^+$ and this will be discussed more in detail later in the text.

In the previous section, the 55-keV transition visible in the planar germanium spectra of delayed γ-ray transitions was mentioned in connection with the $(29/2^-)$ isomeric state. Another delayed 55-keV transition is placed in the level scheme as depopulating the $13/2^+$ bandhead of Band 1 down to the $11/2^-$ member of Band 2 (see Fig. 1).

Our investigation of the prompt coincidences with the transitions depopulating the states above the $I^\pi = 31/2^+$ member of Band 1 (see Fig. 1) in the JUROGAM II coincidence data reveals γ-ray transitions that do not belong to Band 1. Figure 6(b) shows a spectrum of prompt γ rays gated on the 212-keV transition and measured by JUROGAM II. Along with Band 1 transitions, a set of three new transitions with energies of 153, 620, and 624 keV is seen in this spectrum.

Strong γ-ray peaks at energies of 620 and 624 keV, respectively, are also present in the prompt γ-ray spectrum gated with the delayed 457-keV transition in the delayed-prompt γ-γ coincidence matrix [see Fig. 7(a)]. Combined information from the DCO and IPDCO analyses indicates

a stretched $M1$ character for the 153-, 620-, and 624-keV γ-ray transitions. This set of three transitions is attributed to the feeding of the $29/2^+$ isomeric state in ^{195}Bi. All the aforementioned observations resemble the findings for the ^{193}Bi nucleus. As shown in Fig. 6(c), feeding of this isomeric state from de-excitation of Band 1 states is confirmed by presence of the relevant Band 1 transitions in the isomer-tagged prompt γ-ray spectrum gated on the 156-keV transition of Band 1. A time window of 0–5 μs is used for selection of delayed γ rays necessary for isomer tagging. Additionally, neither the 153-keV nor the 624-keV γ-ray transition appears in the 156-keV-gated spectrum. For this reason they must originate from the de-excitation of the $33/2^+$ member of Band 1. Moreover, it is found that the 153- and 624-keV transitions are in prompt coincidence with each other. On the other hand, there is no evidence for the 620-keV transition being in coincidence either with the γ-ray transitions located below the $31/2^+$ member of Band 1 or with the 153- or 624-keV transitions, respectively. On the basis of γ-γ coincidences and energy-sum arguments, both the 620- and 624-keV transitions are placed as directly feeding the $29/2^+$ isomeric state. Based on the energy sum arguments, a 74-keV $M1$ transition being a member of Band 1 must be assumed. This low-energy transition is placed as depopulating the $I^\pi = 29/2^+$ state in Band 1 at an excitation energy of 3123 keV (see Fig. 1). Apparently, the γ-ray peak at 74 keV in the JUROGAM II spectra overlaps strongly with Bi K x-ray peaks, and hence cannot be clearly observed in the current data.

D. Band 2: $h_{9/2}/f_{7/2}$

The yrast negative parity band (Band 2) is observed for the first time in this work. Contrary to the case of ^{193}Bi, no clear evidence for the $7/2^-$ and $9/2^-$ states in the lower part of the band can be found. The main decay out of Band 2 to the $9/2^-$ ground state proceeds via emission of an intense 950-keV $E2$ transition. It bypasses the possible lower-energy transitions depopulating the states below $11/2^-$ member of Band 2.

Gating on the 694-, 833-, and 950-keV transitions in the prompt γ-γ matrix provides clean spectra to allow construction of the level structure of Band 2. Figure 8 shows the transitions forming Band 2. With the statistics of the present experiment, it was possible to establish Band 2 up to spin and parity of $I^\pi = 23/2^-$ and an excitation energy of 2729 keV.

E. Groups A, B, and C

In Fig. 1, a group of positive parity states is placed to the left of Band 1 and assigned as Group A. The corresponding transitions are identified when the 344- and 887-keV transitions are used as gates in the prompt γ-γ coincidence matrix [see, e.g., Fig. 6(a)]. Gating on the 887-keV γ-ray transition is also used in connection with the γ-γ matrix generated from the backed target data, which allows the placement and character of the transitions side-feeding the $13/2^+$ isomeric state to be resolved.

In Fig. 6(a) two strong γ-ray transitions with energies of 391 and 422 keV are seen. Mainly due to their prompt coincidences with the 344-keV transition and high intensities,
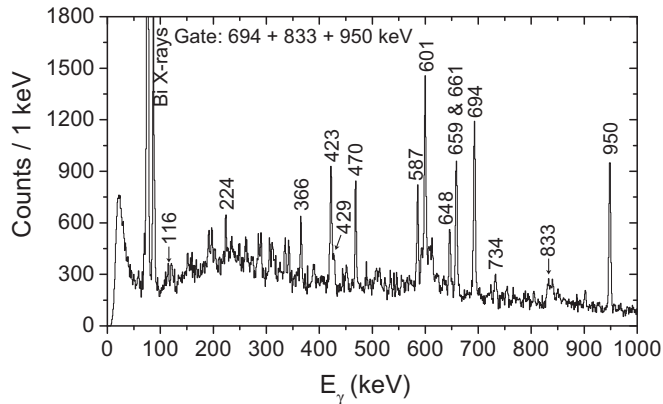
FIG. 8. Sum of the prompt γ-ray spectra gated on the 694-, 833-, and 950-keV transitions. In this spectrum, Band 2 members together with several side-feeding transitions can be seen.

both transitions were previously placed as members of the rotational band built upon the $13/2^+$ isomeric state [11]. Groups B and C include many positive parity states. The strong 391- and 422-keV transitions in Group C were already mentioned in connection with the decay of the $(29/2^-)$ isomeric state. In addition to the dominant 391-keV transition, the 1622-keV state is also depopulated by the 83-keV transition to Band 1 and the 361-keV transition to the 1261-keV state in Group C, as well as to the $15/2^-$ state in Band 2. The $21/2^+$ state at 2044 keV also de-excites to Band 1 via the 507-keV transition. There is also a link from the $27/2^+$ state in Band 1 to the $25/2^+$ state at 2980 keV in Group C via the 67-keV transition. Most of the Group B transitions are of low intensity. Hence, the corresponding levels are presented with tentative spin and parity assignments.

F. Band 3

The yrast $25/2^+$ state located at an excitation energy of 2159 keV has already been mentioned in connection with the decay of both $29/2^-$ and $29/2^+$ isomeric states. Besides this important feature, it is also found to be the lowest state of a bandlike structure (Band 3 in Fig. 1). Band 3 decays solely by the emission of a single 115-keV $E2$ transition to the yrast $21/2^+$ state of Group C. Due to weak coincidences with the 360- and 645-keV intraband transitions, placement of the uppermost state of Band 3 at excitation energy of 4.071 MeV is only tentative and the state is left without a spin and parity assignment.

G. Group D

A group of negative parity states labeled as Group D is placed on the right of Band 2 in the ^{195}Bi level scheme (see Fig. 1). The members of Group D mostly de-excite to Band 2, and in some cases there are also links in the opposite direction. Also placed in Group D are the previously unobserved $7/2^-$ and $9/2_2^-$ states. The 492- and 690-keV $M1$ transitions are identified to depopulate the $7/2^-$ and $9/2^-$ states down to the $9/2^-$ ground state.

The two lowest-lying states of Group D at 1119 and 1199 keV (placed on the left from Band 2 in Fig. 1), respectively,

both de-excite to the $9/2^-$ ground state by a single transition. As there appears to be no signatures of collectivity in Group D, a spherical shape is attributed to these states.

H. Levels and transitions above the isomeric states

The $(29/2^-)$ isomeric state is also identified as a bandhead of a new bandlike structure (Band 4). By gating on the low-energy transitions below this isomeric state in the delayed-prompt γ-γ coincident matrix, transitions feeding the $(29/2^-)$ isomeric state can be identified. Figure 7(b) presents such a γ-ray spectrum measured with JUROGAM II and gated on the delayed 151- and 176-keV transitions. In Fig. 7(b) the transitions forming Band 4 can easily be recognized. The structure of this spectrum proves the assumption that the 454-keV transition is the main feeding transition of the $(29/2^-)$ isomeric state. The assignments of $M1$ and $E2$ characters for most of the Band 4 transitions are in agreement with results of the DCO and IPDCO analyses. In the present study, Band 4 is observed up to $I^\pi = (43/2^-)$ and excitation energy of 4981 keV.

In the level scheme, the $(31/2^-)$ and $(33/2^-)$ members of Band 4 are fed by a level structure labeled as Group F (see Fig. 1). Energy level identification as well as the level ordering within Group F is achieved thanks to strong coincidences with the 575- and 761-keV transitions. Some of the strongest Group F transitions, e.g., with energies of 302, 575, and 761 keV, are visible in Fig. 7(b).

In the analysis of the JUROGAM II events gated on the delayed γ-ray transitions from the de-excitation path of the $(29/2^-)$ isomeric state, a set of transitions forming a structure with characteristics resembling a rotational band (Band 5) is observed. In the same set of JUROGAM II events, a cascade of five coincident low-energy transitions with energies of 169, 196, 229, 268, and 294 keV is found to be in coincidence with the 454-keV transition, and hence to feed the $(29/2^-)$ isomeric state. The 497- and 563-keV $E2$ transitions fix the ordering of the five low-energy γ-ray transitions. As a cascade of $M1$ and $E2$ transitions, they form a bandlike structure Band 6 (see Fig. 1). The current data do not show any transitions linking either Band 5 or Band 6 to Band 4. However, transitions of Bands 5 and 6 are observed in the isomer-tagged JUROGAM II γ-γ coincidence matrix gated on the 454-keV and in some cases even the 434-keV transitions feeding the $(29/2^-)$ isomeric state, and vice versa. It is possible that Band 5 is connected to the isomeric $(29/2^-)$ state directly by the 666- and 672-keV transitions. Alternatively, this connection involves an unobserved, presumably low energy transition. Therefore the lowest members of both bands are placed, even though floating, above an excitation energy of 2381 keV in the level scheme (see Fig. 1). Since Bands 5 and 6 remain floating, level energies together with spins and parities remain undetermined.

Transitions belonging to the level structure feeding the $29/2^+$ isomeric state are present in Fig. 8(a). Along with transitions connecting Band 1 to the $29/2^+$ isomeric state, and members of Band 1, a high-energy 902-keV $E2$ transition is observed in this γ-ray spectrum. The 902-keV $E2$ transition is identified as depopulating the nonyrast $I^\pi = 33/2^+$ state to the $29/2^+$ isomeric state. This transition plays an important role as a building block in constructing the level structure

labeled as Group E built upon the $29/2^+$ isomeric state (see level scheme in Fig. 1).

I. Superdeformation

So far, one superdeformed (SD) band has been reported for ^{195}Bi by Clark *et al.* [5]. Even though the average excitation energies of Bi nuclei produced in Ref. [5] and our experiment were basically identical, we do not see evidence that would confirm the SD band discussed in Ref. [5]. In the recoil-gated triple-γ coincidence JUROGAM II data, a sequence of γ-ray transitions with $\sim$41-keV energy spacings, typical for SD bands in this mass region, appear. The transition energies (see the bottom part of Table III) are comparable to those for the SD band in ^{193}Bi [3] and the favored signature SD band in ^{191}Bi [1]. Unlike the neighboring lighter Bi nuclei, the possibilities to use the RDT technique are significantly limited due to the long α-decay half-lives of the $9/2^-$ ground state and the $1/2^+$ intruder state. Coupled with the low transition intensities in the recoil-gated data, the multipolarities and electromagnetic character of the transitions in the cascade cannot be resolved.

IV. DISCUSSION

Due to the position of the ^{195}Bi isotope in the chart of nuclei, which is eight neutrons away from the β-stability line, until now the ^{195}Bi nucleus was believed to possess very little collectivity. In comparison, the ^{193}Bi isotope is a textbook example of a transitional nucleus. It is located between the lighter Bi isotopes dominated by deformed structures, and the heavier isotopes, in which the yrast structures can be explained assuming a spherical shape. This gives rise to a high probability of finding both collective oblate and spherical structures in ^{193}Bi. In the following section, we present the experimental data exhibiting an extensive manifestation of shape coexistence in the ^{195}Bi nucleus. The admixture of structures specific for this nuclear phenomenon is assumed to be the explanation for the richness of the level structures observed in the ^{195}Bi isotope. Several mostly bandlike level structures will be discussed. Coupling of an unpaired proton to the semimagic lead core is debated and used for the description of majority of these bands. At the same time, explanations in terms of aligned angular momenta i_x and comparisons of experimental $B(M1)/B(E2)$ ratios with theoretical predictions [30,31] will be proposed. We also point out the fact that some observed bands could be treated as shears bands.

In Fig. 9, the systematic behavior of the energies of selected yrast states in neutron-deficient odd-A Bi isotopes are shown. Many of these states have isomeric character, dependant on the neutron number. From the figure it is noticeable that changes in configurations need to be considered for the $17/2^+$ and $21/2^+$ states when ^{195}Bi is reached. Another feature to be noted is the "inverted" parabola-shape-like behavior of the $29/2^+$ and $29/2^-$ states. These parabolas seem to cross two times, signaling almost identical excitation energies in two particular isotopes, ^{193}Bi and ^{203}Bi. This is a very interesting observation, since as is shown later in the text, these two states are associated with completely different three quasiparticle configurations.
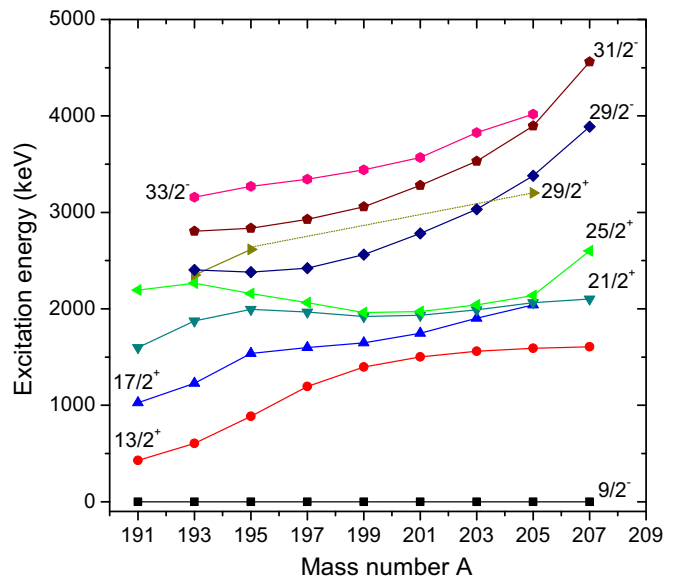

FIG. 9. Systematics of selected excited states in odd-A Bi isotopes. Where the exact excitation energy is not known due to unobserved low-energy transitions Δ, it is set to 40 keV for clarity. The data are taken from [32,33] (^{197}Bi), [34] (^{199}Bi), [34,35] (^{201}Bi), [36–38] (^{203}Bi), [37–39] (^{205}Bi), [40–42] (^{207}Bi), and for ^{193,195}Bi from [3] and the present study.

A. Low-lying collective structures

1. $\pi i_{13/2}$ band

Systematic studies of nuclei in the mass region of the present study show that sudden lowering of the $13/2^+$ level energies occurs in the chain of neutron-deficient Bi isotopes. This is schematically shown in Fig. 9, as can be attributed to the interaction of the $i_{13/2}$ proton with increasing number of neutron holes. Hence, this effect is more profound in the very neutron-deficient nuclei close to neutron midshell. As can be easily seen in Fig. 9, the decrease of the $13/2^+$ level energies is especially apparent for the $A = 191$–195 Bi isotopes. In those odd-A Bi nuclei, the $13/2^+$ states feature an isomeric character. In fact, the $13/2^+$ isomeric states in the neutron-deficient bismuth nuclei with $A < 199$ can be understood as the coupling of an $i_{13/2}$ proton to the oblate $2p$-$2h$ 0^+ intruder state of the neighboring even-even Pb core. Quite recently, strongly coupled rotational bands built upon the $13/2^+$ isomeric states have been identified in ^{191,193,195}Bi isotopes [1–3].

The smoothly increasing behavior of the transition energies of the strongly coupled band in ^{195}Bi built upon the $13/2^+$ isomeric state terminates when the $I^\pi = 25/2^+$ state is reached. In Fig. 10, the measured aligned angular momenta i_x as a function of rotational frequency for the $i_{13/2}$ band in ^{195}Bi are shown. Note that a sharp band crossing takes place in ^{195}Bi at exactly the same crossing frequency of $\hbar\omega \sim 0.2$ MeV as in ^{193}Bi [3], with a gain in alignment of 10–11$\hbar$. To analyze and describe this behavior of Band 1 in ^{195}Bi, the explanation given in [3] is adopted saying that such a gain in alignment may be attributed to alignment of the two $i_{13/2}$ neutrons. Sharp $i_{13/2}$ neutron alignments seem to be rather common for
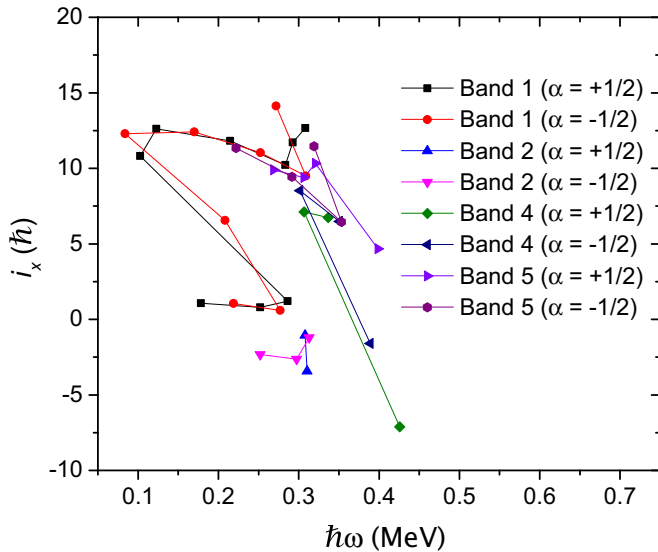
FIG. 10. Aligned angular momenta i_x for the favored ($\alpha = +1/2$) and unfavored ($\alpha = -1/2$) signatures of Band 1 ($\pi 13/2^+[606]$), Band 2 ($\pi 7/2^-[514]$), Bands 4 and 5 in ^{195}Bi. A reference with the Harris parameters $J_0 = 13\hbar^2/$MeV and $J_1 = 219\hbar^4/$MeV^3 taken from [3] has been subtracted.

nuclei with low and moderate oblate deformations in this mass region. Deformation and triaxiality in the neighboring ^{191,193}Bi isotopes have been evaluated by means of total Routhian surface (TRS) calculations by Nieminen *et al.* [2]. In order to support the claim concerning the alignment of two $i_{13/2}$ neutrons, both experimental and theoretical $B(M1)/B(E2)$ ratios are plotted in Fig. 11(a) for Band 1 in ^{195}Bi. If the aforementioned similarities between Band 1 in ^{193}Bi and ^{195}Bi are included in the theoretical calculation, it is apparent that the calculation nicely follows the trend given by experimental values below the band crossing also in ^{195}Bi. At higher rotational frequencies, experimental $B(M1)/B(E2)$ ratios may indicate that above the band crossing the $i_{13/2}$ band is not as regular (or collective) as smooth increase of level energies suggests.

2. $\pi(f_{7/2}/h_{9/2})$ band

Two different configurations may be attributed to the yrast negative parity band labeled as Band 2 in ^{195}Bi. First, it can be associated with the 7/2[514] Nilsson configuration (mixed $h_{9/2}/f_{7/2}$). Second, since the connection between Band 2 and the $7/2^-$ state is not established, another option is that Band 2 could in fact correspond to a band based on the 9/2[550] proton orbital in ^{193}Bi [3]. Limited information obtained for Band 2 and displayed in Fig. 10 and Fig. 11(b), respectively, does not allow for the experimental values to be compared to those for
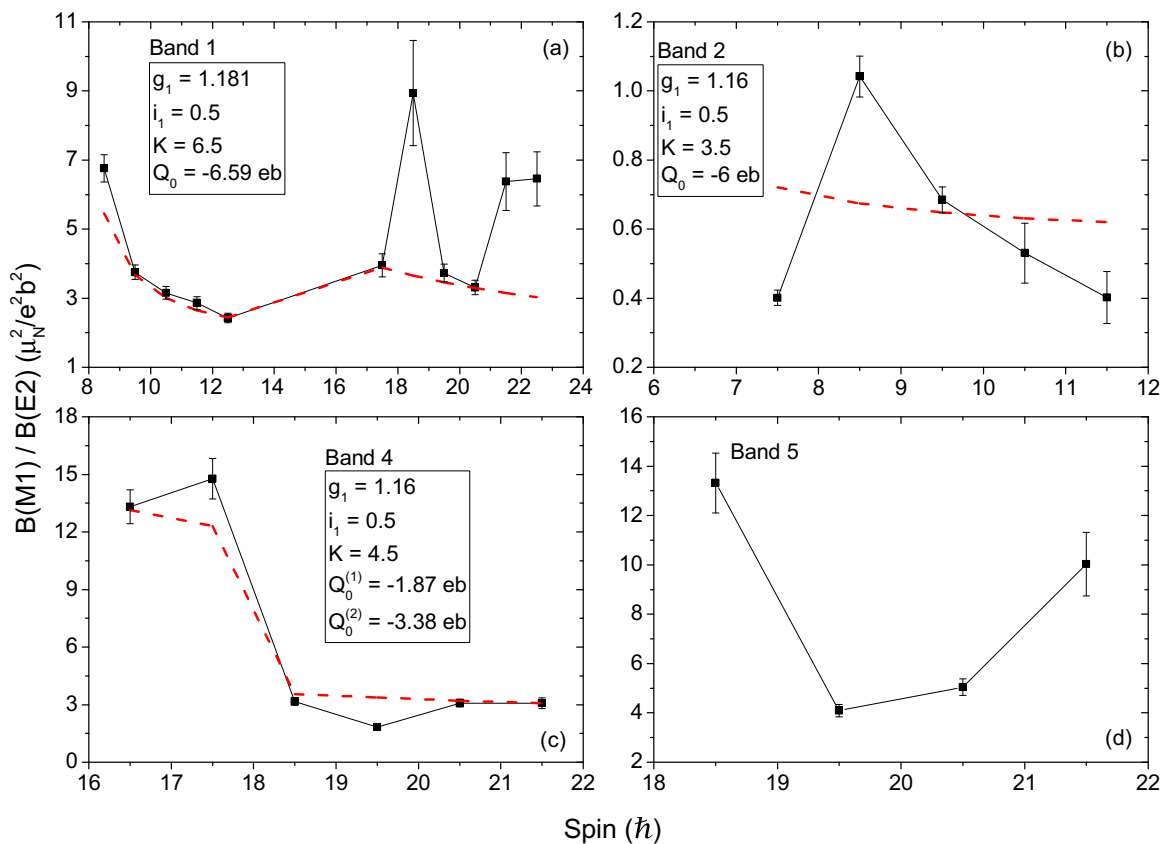

FIG. 11. Experimental $B(M1)/B(E2)$ ratios for (a) Band 1, (b) Band 2, (c) Band 4, and (d) Band 5 in ^{195}Bi, together with semiempirical estimates for the first three bands indicated by dashed red line. The parameter values for the odd proton used in the calculations are indicated. Parameters g_1 and i_1 are taken from [2].

^{193}Bi. In this case, no major conclusions on the behavior of Band 2 can be made. The uppermost state with $I = 23/2$ is found to be insufficient for two-neutron alignment, as shown in Fig. 10. Moreover, the smooth increase of the $E2$ transition energies, typical for rotational bands, is not followed in the case of the favored signature of Band 2. As a consequence, sudden changes in evolution of $i_x(\omega)$ can be noticed. This together with the rather scattered values of experimental $B(M1)/B(E2)$ ratios [see Fig. 11(b)] can be understood as a result of strong mixing of Band 2 and Group D states, especially at lower spins. Additionally, it is not clear whether the $7/2^-$ and $9/2_2^-$ states are spherical or whether they in fact belong to oblate-deformed Band 2.

B. High-spin isomeric states

The existence of high-spin isomeric states in the odd-A neutron-deficient Bi isotopes has been proven in the range $193 \leqslant A \leqslant 207$. Systematic studies show that certain high-spin isomeric states, which are present in heavier Bi nuclei, become short-lived yrast states in their lighter odd-A neighbors (e.g., the $21/2^+$ and $25/2^+$ states). On the other hand, including the observations of the present study, the $(29/2^-)$ state is found to keep its isomeric character in all neutron-deficient odd-A Bi nuclei from ^{207}Bi down to ^{193}Bi. As in ^{193}Bi, the $(29/2^-)$ isomeric state in ^{195}Bi can be understood as the $\pi h_{9/2}$ coupled to the $(i_{13/2}^{-2})_{12^+}$ isomeric state in the Pb core, and the same interpretation also applies for the $(31/2^-)$ and $(33/2^-)$ members of Band 4. Another feature common for both odd-A Bi isotopes is the decay patterns of the $(29/2^-)$ isomeric states, where a single low-energy $E2$ transition depopulates this isomeric state to the $25/2^-$ state. Interestingly, this state also carries an isomeric character in ^{195}Bi. The $\pi h_{9/2} \otimes \text{Pb}_{10^+}$ configuration is assigned for the $25/2^-$ state. Together with other decay paths, it is also depopulated by a 90-keV transition to the $21/2^-$ state with a deduced $\pi h_{9/2} \otimes \text{Pb}_{8^+}$ configuration. From the current data a reduced transition strength $B(E2, 90 \text{ keV}) = 0.39(8)$ W.u. is obtained. Even though the information about the corresponding $10^+ \rightarrow 8_2^+$ transition in ^{194}Pb is limited, the $B(E2, 90 \text{ keV})$ value is slightly hindered when compared to the reduced transition strength of ~ 1 W.u. for the corresponding 61-keV transition in ^{192}Pb.

Regarding the half-life of the $(29/2^-)$ isomeric state, the $T_{1/2}$ value is shorter by a factor of ~ 5 in ^{195}Bi when compared to its odd-A neighbor ^{193}Bi. This is also reflected in the deduced transition strengths. Even though the energies of the $E2$-type transitions depopulating the $(29/2^-)$ isomeric states in ^{193,195}Bi are almost equal, the corresponding reduced transition strength $B(E2) = 0.255(5)$ W.u. in ^{195}Bi is five times larger than $B(E2) = 0.052(2)$ W.u. in ^{193}Bi [3]. The experimentally measured $B(E2)$ value seems to be slightly hindered when compared to 0.466 W.u. for the corresponding $12^+ \rightarrow 10^+$ transition in ^{194}Pb [43], but as we present in Fig. 12, it nicely continues in the gradually increasing trend given by the experimental values of the Pb isotones.

In the case of Band 4 built upon the $(29/2^-)$ isomeric state (see Fig. 1), the same quasiparticle (qp) configuration is assigned to this band as for Band 2 after the neutron $i_{13/2}$
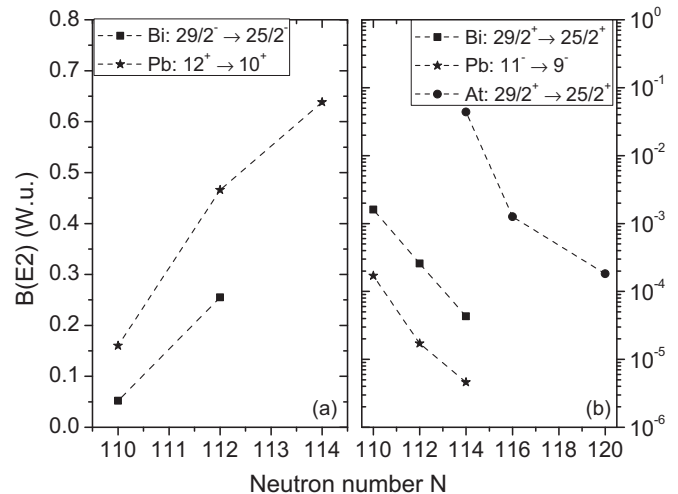

FIG. 12. Experimental $B(E2)$ values for (a) the transitions de-populating the $29/2^-$ isomeric states in ^{193,195}Bi [3], and $12^+ \rightarrow 10^+$ core transitions in ^{192}Pb [45] and ^{194}Pb [43], respectively, and (b) the $29/2^+ \rightarrow 25/2^+$ transitions in ^{193,195}Bi [3], $11^- \rightarrow 9^-$ transitions in ^{192}Pb [45], ^{194}Pb [43], ^{196}Pb [46] isotopes, and the $29/2^+ \rightarrow 25/2^+$ transitions in ^{199}At [47], ^{201}At [48,49] and ^{205}At [50] isotopes. Data for ^{195}Bi are from the present work. Consider the very fine scale of the y axis of panel (b).

alignment. The i_x values for Band 4 are also shown in Fig. 10. Even though the data points for Band 2 are not representative, i_x of Band 4 can be compared to i_x of the unfavored signature of Band 2. The same gain in alignment of about $10\hbar$ is observed, which was previously attributed to the alignment of two $i_{13/2}$ neutrons. When the qp configuration is taken into account, we need to assume almost spherical shape for the few lowest members of Band 4. In Fig. 11(c) the experimental $B(M1)/B(E2)$ ratios for Band 4 are shown. In order to be able to explain their observed behavior as a function of spin, it is needed to consider a shape change within the band. In Fig. 11(c), the nuclear shape adjustments are represented by two different values of quadrupole moments labeled as $Q_0^{(1)}$ and $Q_0^{(2)}$. The superscripts (1) and (2) indicate the regions of spin values to which a certain Q_0 value is applied, and the figure is split accordingly. Following the experimental data, an indication of Band 4 becoming more rotational-like with increasing spin can be seen. This is also represented by a lowering of the intraband transition energies (see Fig. 1). As a summary, data shown in Figs. 10 and 11 may indicate that the nuclear shape associated with this $\pi h_{9/2} \otimes \nu i_{13/2}^2$ built level structure evolves towards an oblate shape with increasing spin. However, there is another band in the level scheme, Band 5, which may also be assigned with the same configuration at oblate shape. It would be interesting to see whether there are connections to Band 2 from the uppermost levels of Band 4 in ^{195}Bi. This remains to be seen in the future experiments.

Prior to the present study, the existence of the $29/2^+$ state has been reported in only two odd-A neutron-deficient bismuth isotopes, namely ^{193}Bi and ^{205}Bi (see Fig. 9). Nonetheless, only the $29/2^+$ state in ^{193}Bi has been assigned with an isomeric character. Observation of the $29/2^+$ isomeric state in ^{195}Bi

TABLE IV. Reduced transition strengths $B(E1)$ for the selected transitions in ^{195}Bi and the corresponding core transitions in ^{194}Pb. The data for ^{194}Pb are taken from [46] (305.0-keV transition), and [51] (173.7-keV transition).

^{195}Bi transition	$B(E1)$ (W.u.)	^{194}Pb transition	$B(E1)$ (W.u.)
$29/2^+ \rightarrow 29/2^-$	235.8 keV: $5.91(62) \times 10^{-10}$	$11^- \rightarrow 12^+$	305.0 keV: $2.40(15) \times 10^{-8}$
$25/2^- \rightarrow 25/2^+$	176.0 keV: $5.03(60) \times 10^{-8}$	$10^+ \rightarrow 9^-$	
$25/2^- \rightarrow 23/2^+$	55.0 keV: $2.86(34) \times 10^{-7}$	$10^+ \rightarrow 9^-$	173.7 keV: $2.02(7) \times 10^{-6}$
$25/2^- \rightarrow 23/2^+$	150.6 keV: $3.41(41) \times 10^{-7}$	$10^+ \rightarrow 9^-$	

thus signifies an important input for the systematics of the high-spin isomeric states in the neutron-deficient Bi nuclei. In a similar manner to ^{193}Bi, the $\pi i_{13/2} \otimes [\pi h_{9/2}^2]_{8^+}$ configuration is attributed to the $29/2^+$ isomeric state in ^{195}Bi. Looking at Fig. 9, it can be seen that with the information available at the time of this study the $29/2^+$ level energies follow the trend given by the $13/2^+$ level systematics.

Concerning the decay of the $29/2^+$ isomeric state, reduced transition strengths $B(E2) = 2.57(4) \times 10^{-4}$ W.u. and $B(E1) = 5.9(1) \times 10^{-10}$ W.u. are deduced for the 457-keV $E2$ and 236-keV $E1$ transitions, respectively. It is worth repeating that the dominant 457-keV transition depopulates the $29/2^+$ isomeric state ($\pi[i_{13/2}h_{9/2}^2]$) to the $25/2^+$ state ($\pi h_{9/2} \otimes \nu[f_{5/2}^{-1}i_{13/2}^{-1}]$). Regarding the $E2$-type transitions, $B(E2, 457$ keV) is hindered in comparison to $B(E2) = 1.6 \times 10^{-3}$ W.u. for the corresponding $11^- \rightarrow 9^-$ transition in ^{194}Pb [43] (^{194}Pb: $\pi[h_{9/2}i_{13/2}]_{11^-}$ and $\nu[f_{5/2}^{-1}i_{13/2}^{-1}]_{9^-}$ [44]). Nevertheless, as is shown in Fig. 12(b), a decreasing trend of $B(E2)$ values as a function of neutron number N is apparent for odd-A Bi isotopes, and similarly to the $(29/2^-)$ isomeric states, they also nicely follow the trend in the Pb core isotopes. For comparison, the experimental $B(E2)$ values so far reported for the $(29/2^+)$ isomeric states in a few odd-A neutron-deficient At isotopes are presented (see [48] and references therein).

The level energy differences (ΔE) between the $29/2^+$ and $13/2^+$ isomeric states in ^{193}Bi and ^{195}Bi are 1745 and 1729 keV, respectively. In ^{197}Bi an isomeric state at an excitation energy of 2928 keV with tentative spin and parity assignment of $(31/2^-)$ has been reported [32,33]. This state is located 1732 keV above the $i_{13/2}$ $13/2^+$ state. For the relevant 864-keV transition depopulating this isomeric state, assuming an $E2$ character and partial half-life of 400 ns, a value $B(E2, 864$ keV) $= 4.3(6) \times 10^{-5}$ W.u is obtained. Such a $B(E2)$ value would fit well into the slowly decreasing trend of $B(E2)$ values, plotted for the selected Bi and Pb isotopes in Fig. 12(b). To conclude, the isomeric state at 2928 keV in ^{197}Bi may actually correspond to the $29/2^+$ isomeric states observed in ^{193,195}Bi nuclei.

$B(E1)$ values for the transitions depopulating the $29/2^+$ and $25/2^-$ isomeric states, together with their even-even Pb counterparts, are listed in Table IV. From this table it is apparent that also here the transitions are hindered when compared to even-even Pb. Nevertheless, a systematic upward trend with decreasing spin can be observed.

Regarding the level structure (Group E) feeding the $29/2^+$ isomeric state (see Fig. 1), one thing to notice is the parity change for several energy levels, starting at $I^\pi = 39/2^-$. These negative parity states of Group E most likely arise

from coupling the configuration of the $29/2^+$ isomeric state state to the 7^- and 9^- core states ($\nu i_{13/2}p_{3/2}$ and $\nu i_{13/2}f_{5/2}$ configurations) [52,53].

Remarkable similarities are found not only in the feeding patterns of the $29/2^+$ isomeric states in ^{193}Bi and ^{195}Bi, but also in the mixing of the two closely lying $31/2^+$ states of Band 1 and Group E. Assuming a simple two-state mixing model and following the same procedure as in [3], the experimental ratio of $B(M1)$ transition strengths is evaluated to be $\frac{B(M1,153)}{B(M1,156)} = 0.193$, which gives the following mixing amplitudes: $\alpha = 0.92$ and $\beta = 0.40$. This implies an interaction energy of 1.1 keV and corresponds to an energy shift of $0.239 \Delta E_u$ between the perturbed and unperturbed $31/2^+$ level energies. Assuming experimentally observed perturbed splitting $\Delta E_p = 3$ keV, an unperturbed splitting $\Delta E_u = 2.03$ keV is extracted from the experimental data. These results are in accordance with the assumption of very weak mixing of states built on different three-qp configurations.

C. Bands 3, 5, 6 and Group F

Similarly to Band 4, a sign of collectivity also appears in Band 3. A proposed configuration would be an $h_{9/2}$ proton coupled to the 9^- Pb-core state. It should be noted that recent TRS calculations [12] predict an essentially spherical shape for such a configuration.

In the ^{195}Bi level scheme shown in Fig. 1, Band 5 is left floating, due to observed coincidences in the isomer-tagged spectrum. In the following discussion it is assumed that the 666- and 672-keV transitions directly feed the $(29/2^-)$ isomeric state, and that $i = 29/2^-$. In Fig. 10 the evolution of aligned angular momenta for Band 5 can be seen. Experimental $B(M1)/B(E2)$ ratios are shown in Fig. 11(d). One alternative is that Band 5 is based on the $\pi i_{13/2} \otimes \nu i_{13/2}(p_{3/2}/f_{5/2})$ configuration (option 1). This configuration has been attributed to Band 3 in ^{193}Bi [3]. Another explanation for Band 5 is that it is the continuation of Band 2 after the $i_{13/2}$ neutron alignment (option 2). Assuming small deformations both of these configurations can give $B(M1)/B(E2)$ ratios similar to the experimental values for $I = 19.5\hbar$ and $20.5\hbar$ in Fig. 11(d). Note that the first data point in this figure is probably affected by the mixing of two states with the same angular momentum near the bottom of the band. Considering the first alternative (option 1), especially at lower spins, Band 5 in ^{195}Bi and Band 3 in ^{193}Bi have quite different level patterns and their decay paths do not resemble each other. Additionally, aligned angular momentum displayed in Fig. 10 is too large to be in agreement with this qp configuration. On the other hand, the extracted aligned angular momenta for Band 5 are consistent with option

2. Band 5 crosses Band 2 in the range $\hbar\omega \approx 0.20$–0.22 MeV, which is similar to the band-crossing frequency observed in the proton $i_{13/2}$ band (Band 1). Therefore, Band 5 could be a continuation of the $f_{7/2}/h_{9/2}$ band (Band 2) after the sharp $i_{13/2}$ neutron alignment.

In the case of the floating Band 6, there is insufficient data for a reliable $i(x)$ or $B(M1)/B(E2)$ ratio analysis. Since coincidences between some members of Band 6 and at least 454- and 434-keV transitions (Band 4) are observed, the Band 6 bandhead should have a spin higher than the few lowest levels of Band 4. Therefore, Band 6 is likely to be built on a five-qp configuration.

In fact, Band 6 or a bandlike regular sequence of $M1$ transitions in Group F (further only Group F) may be counterparts of magnetic rotational Band 1 in ^{194}Pb [54]. Especially Group F turns out to be a good shears band candidate, due to no $E2$ transitions observed. The $(35/2^-)$ state at 3595 keV is assumed to be the bandhead state. Group F de-excites to the $(29/2^-)$ isomeric state. In Ref. [54] Band 1 in ^{194}Pb was found to feed the 12^+ isomeric state. Closer inspection tells us that the energy difference between the bandheads and corresponding isomeric states (11^- in ^{194}Pb and $29/2^+$ in ^{195}Bi) is several hundreds keV less in ^{195}Bi. One explanation can be the interaction of neutrons with an extra $h_{9/2}$ proton in the configuration of Band 1 in ^{194}Pb. Owing to comparisons just made here, we propose the $\pi h_{9/2}^2 i_{13/2} \otimes \nu i_{13/2} p_{3/2}$ five-qp configuration for a shears band in ^{195}Bi.

D. Superdeformation

The SD band candidate observed in the current study is similar to the SD bands in ^{191,193}Bi [1,3]. Those bands predominantly decay to the $1/2^+$ intruder state. In ^{195}Bi the RDT technique could not be used due to the long half-life. Therefore, decay from the SD band to the $1/2^+$ intruder state could not be identified. Due to the aforementioned similarities between the SD bands, a configuration where a proton occupies the prolate-deformed $i_{11/2}1/2^+[651]$ Nilsson orbital is also assigned to the SD band in ^{195}Bi. In Ref. [5] an identical SD band was assigned to ^{196}Bi, where in addition to an odd proton in the 1/2[651] orbital, also a strongly rotation-aligned neutron is coupled to the even-Pb SD core.

E. Noncollective states

It is not easy to explain the existence of many experimentally observed states in ^{195}Bi, but a relatively easy explanation can be given for at least several yrast states. Some of the positive parity states belonging to Group C (see Figs. 1) can

be interpreted by the coupling of the odd proton in the $h_{9/2}$ orbital to spherical negative parity core states in ^{194}Pb. From the theoretical point of view, an approach called the cluster interaction was used for this purpose in the past [32,34]. The systematic behavior of these states is presented in Fig. 9. The second $13/2^+$ state at excitation energy of 1261 keV (see Fig. 1) can be understood as a proton occupying the spherical $i_{13/2}$ orbital. By looking at Fig. 9, it can be seen that the excitation energy of the spherical $13/2_2^+$ state is similar to the energies of the $13/2^+$ states in heavier odd-A Bi isotopes. Furthermore, the second $I^\pi = 13/2^-$ state placed at 1199 keV in the current level scheme (see Fig. 1) is attributed to the coupling of an $\pi h_{9/2}$ to a spherical ^{194}Pb$_{2+}$ core state.

V. CONCLUSION

In summary, many excited states in ^{195}Bi have been observed using various tagging techniques. The previously known level scheme was considerably extended and revised. New levels and band structures were observed. An oblate deformation had to be assumed in order to understand several rotational structures, whereas other structures require interpretation in terms of a spherical shape. A new high-spin isomeric state with a spin and parity of $29/2^+$, associated with a $\pi(i_{13/2}h_{9/2}^2)$ configuration, was found and two decay paths were identified. The 457-keV $E2$ transition carrying most of the intensity feeds the $25/2^+$ state of $\pi h_{9/2} \otimes \nu(i_{13/2}^{-1}f_{5/2}^{-1})$ origin. In the second decay path, the 236-keV $E1$ transition depopulates the $29/2^+$ isomeric state down to the $(29/2^-)$ isomeric state. Decay of the $(29/2^-)$ isomeric state proceeds via emission of the 46-keV γ ray, which feeds the $25/2^-$ isomeric state with a half-life of 80 ns. The $(29/2^-)$, $25/2^-$, and the $21/2^-$ states connected by low-energy $E2$ transitions form a part of the $\pi h_{9/2} \otimes \nu i_{13/2}^{-2}$ multiplet. Candidates for a shears band and superdeformed band were observed. In this study, remarkable similarities were observed between ^{195}Bi and the recently studied isotope ^{193}Bi. It would be interesting to investigate whether or not the oblate band built upon the $13/2^+$ state also exists in ^{197}Bi.

ACKNOWLEDGMENTS

[1] M. Nyman *et al.*, Eur. Phys. J. A **51**, 31 (2015).

[2] P. Nieminen *et al.*, Phys. Rev. C **69**, 064326 (2004).

[3] A. Herzáň *et al.*, Phys. Rev. C **92**, 044310 (2015).

[4] R. M. Clark *et al.*, Phys. Rev. C **51**, 1052(R) (1995).

[5] R. M. Clark *et al.*, Phys. Rev. C **53**, 117 (1996).

[6] D. P. McNabb *et al.*, Phys. Rev. C **53**, 541(R) (1996).

[7] M. S. Johnson *et al.*, Phys. Rev. C **71**, 024317 (2005).

[8] W. Nazarewicz, R. Wyss, and A. Johnson, Nucl. Phys. A **503**, 285 (1989).

[9] W. Satula, S. Cwiok, W. Nazarewicz, R. Wyss, and A. Johnson, Nucl. Phys. A **529**, 289 (1991).

[10] T. Lönnroth *et al.*, Phys. Rev. C **33**, 1641 (1986).

[11] H. Pai *et al.*, Phys. Rev. C **85**, 064317 (2012).

[12] T. Roy *et al.*, Eur. Phys. J. A **51**, 153 (2015).

[13] G. Duchene *et al.*, Nucl. Instrum. Methods Phys. Res., Sect. A **432**, 90 (1999).

[14] C. W. Beausang *et al.*, Nucl. Instrum. Methods Phys. Res., Sect. A **313**, 37 (1992).

[15] C. Rossi Alvarez, Nucl. Phys. News **3**, 10 (1993).

[16] A. Georgiev and W. Gast, IEEE Trans. Nucl. Sci. **40**, 770 (1993).

[17] M. E. Leino *et al.*, Nucl. Instrum. Methods Phys. Res., Sect. B **99**, 653 (1995).

[18] J. Sarén *et al.*, Nucl. Instrum. Methods Phys. Res., Sect. A **654**, 508 (2011).

[19] R. D. Page *et al.*, Nucl. Instrum. Methods Phys. Res., Sect. B **204**, 634 (2003).

[20] I. H. Lazarus *et al.*, IEEE Trans. Nucl. Sci. **48**, 567 (2001).

[21] C. Scholey *et al.*, Phys. Rev. C **63**, 034321 (2001).

[22] P. Rahkila, Nucl. Instrum. Methods Phys. Res., Sect. A **595**, 637 (2008).

[23] D. C. Radford, Nucl. Instrum. Methods Phys. Res., Sect. A **361**, 297 (1995).

[24] D. C. Radford, Nucl. Instrum. Methods Phys. Res., Sect. A **361**, 306 (1995).

[25] E. Coenen *et al.*, Phys. Rev. Lett. **54**, 1783 (1985).

[26] K. H. Schmidt *et al.*, Phys. Lett. B **168**, 39 (1986).

[27] K. S. Krane, R. M. Steffen, and R. M. Wheeler, Nucl. Data Tables **11**, 351 (1973).

[28] K. Starosta *et al.*, Nucl. Instrum. Methods Phys. Res., Sect. A **423**, 16 (1999).

[29] T. Kibedi *et al.*, Nucl. Instrum. Methods Phys. Res., Sect. A **589**, 202 (2008).

[30] S. Frauendorf, Phys. Lett. B **100**, 219 (1981).

[31] F. Dönau, Nucl. Phys. A **471**, 469 (1987).

[32] T. Chapuran *et al.*, Phys. Rev. C **33**, 130 (1986).

[33] G. K. Mabala *et al.*, Eur. Phys. J. A **25**, 49 (2005).

[34] W. F. Piel, Jr. *et al.*, Phys. Rev. C **31**, 2087 (1985).

[35] R. Broda *et al.*, Nucl. Phys. A **389**, 366 (1982).

[36] H. Hübel *et al.*, Nucl. Phys. A **294**, 177 (1978).

[37] T. Lönnroth, Z. Phys. A **307**, 175 (1982).

[38] H. Hübel *et al.*, Z. Phys. A **314**, 89 (1983).

[39] R. Brock *et al.*, Nucl. Phys. A **278**, 45 (1977).

[40] I. Bergström *et al.*, Phys. Rev. **181**, 1642 (1969).

[41] T. Lönnroth and B. Fant, Phys. Scr. **18**, 172 (1978).

[42] T. Lönnroth, J. Blomqvist, I. Bergström, and B. Fant, Phys. Scr. **19**, 233 (1979).

[43] M. Kaci *et al.*, Nucl. Phys. A **697**, 3 (2002).

[44] K. Vyvey *et al.*, Phys. Rev. C **69**, 064318 (2004).

[45] A. J. M. Plompen *et al.*, Nucl. Phys. A **562**, 61 (1993).

[46] G. D. Dracoulis *et al.*, Phys. Rev. C **72**, 064319 (2005).

[47] U. Jakobsson *et al.*, Phys. Rev. C **82**, 044302 (2010).

[48] K. Auranen *et al.*, Phys. Rev. C **91**, 024324 (2015).

[49] K. Auranen *et al.*, Phys. Rev. C **92**, 039901(E) (2015).

[50] R. F. Davie *et al.*, Nucl. Phys. A **430**, 454 (1984).

[51] B. Singh, Nucl. Data Sheets **107**, 1531 (2006).

[52] K. Helariutta *et al.*, Eur. Phys. J. A **6**, 289 (1999).

[53] J. M. Lagrange *et al.*, Nucl. Phys. A **530**, 437 (1991).

[54] T. Kutsarova *et al.*, Phys. Rev. C **79**, 014315 (2009).